Earth Systems, Resources, and Sustainability, 2026, 1(2), 202–220

Scilight

Earth Systems, Resources, and Sustainability

Journal Homepage: https://www.sciltp.com/journals/esrs

Article

Geochemistry and Petrology of Crust and Mantle Xenoliths and Xenocrysts in the Trans-Khamar-Daban Zone

Igor Ashchepkov[1,2,*], Andrey Tsygankov[2], Galina Burmakina[2], Theodoros Ntaflos[3], Sergey Rasskazov[4], Irina Chuvashova[4] and Yuseff Ailow[5]

[1] Sobolev V.S. Institute of Geology and Mineralogy SB RAS, Novosibirsk 630090, Russia
[2] Dobretsov Geological Institute of Siberian Branch of Russian Academy of Sciences, Ulan-Ude 670047, Russia
[3] Department of Lithospheric Research, University of Vienna, Althanstr. 14, 1090 Wien, Austria
[4] Institute of Earth Crust of Siberian Branch of Russian Academy of Sciences, Irkutsk 664033, Russia
[5] Department of Geology, Al Furat University, Deir ez-Zor, Syria
[*] Correspondence: igor.ashchepkov@igm.nsc.ru

ABSTRACT

The volcanic rocks from Cenozoic Trans-Khamar-Daban volcanic zone (TKDVZ) in Russia and their xenocrysts and crust-mantle xenoliths were investigated by electron microprobe (EPMA) and laser-ablation inductively coupled mass-spectrometry (LA ICP MS) and other methods. They were used to show the composition and reconstructions of structure of the crust and mantle. Volcanism started from Central Part of ridge at 23 Ma and distributed to the shoulders (18–16 Ma) rift margins (13–16 Ma) and top of volcanoes (12–10 Ma), followed by rift valleys (5–2 Ma) and culminated in cinder cones volcanoes (0.8–0.15 Ma). Lavas evolved from sub-alkali to alkaline basalts and tephrites. Lherzolitic xenoliths are nearly primitive, having relics of garnets and simplectites which represent the material of mantle diapirs. The volcanics from Tunka and Dzhida valleys carry abundant cumulate xenoliths related to 2.0–1.0 GPa. The geothermal regimes reconstructed using electron probe (EPMA) mineral analyses and mineral thermobarometry is close to the South-Eastern Australian Geotherm (SEA). At the first stage, it shows heating to 1350 °C near Baikal Lake (Sukhoy volcano). The trace elements in the lherzolites are close to primitive mantle being more depleted near Tunka valley and showing ancient subduction related depletion and hydration in Dzhida. The cumulates show fractionation trends for pyroxenes, garnets amphiboles. The megacrysts show high La/Yb ratios increasing with Fe# for clinopyroxenes and garnets and LILE enrichments for amphiboles and Ti-biotites. The volcanism was caused by deep plume generated with the influence of the subduction from the Pacific and correlated with the events of India- Eurasia collision.

ARTICLE INFO

History:

Received 19 November 2025
Revised 21 February 2026
Accepted 3 March 2026
Published: 11 March 2026

Keywords:

mantle plume;
volcanism;
xenoliths;
geochemistry;
geotherms

Citation:

Ashchepkov, I.; Tsygankov, A.; Burmakina, G.; et al. Geochemistry and Petrology of Crust and Mantle Xenoliths and Xenocrysts in the Trans-Khamar-Daban Zone. *Earth Systems, Resources, and Sustainability* **2026**, *1*(2), 202–220. https://doi.org/10.53941/esrs.2026.100013

Research Highlights

- Cenozoic volcanism and mantle in Trans-Khamar-Daban zone developed in 5 stages 23–0.25 Ma.
- Mantle xenoliths are primitive heated to SEA geotherm, relics of pyropes suggest diapir upwelling.
- Trace elements suggest carbonatite influence and ancient hydration.

1. introduction

In this paper we are discussing the composition and deep mantle-crust structure of Trans Khamar-Daban volcanic zone reconstructed by the material of deep seated xenoliths and xenocysts from Miocene-Quaternary basaltic lavas.

In the late Cenozoic, plume basalt magmatism manifested over a vast area of Eurasia [1] and other regions of the world. In the east [2, 3] and northeast of Asia [4, 5] in the Western Pacific segment [6], it is spatially conjugated with modern and ancient subduction zones [7–9] (Figure 1). The chain of Cenozoic plateau basalts stretching from Primorye [9] through the Tokinsky Stonovik [10, 11], Udokan [11], Vitim plateau [12–18], Khamar-Daban [19], Dzhida Valley [20] Eastern Sayan to Tuva [21] traces the boundaries of microplates to the north of the closure zone of the Mongolian-Okhotsk Ocean [22].

Within Transbaikalia and Mongolia, the thickness of the lithosphere varies according to geophysical data [23]. Basalt fields within Transbaikalia are localized mainly along the boundaries of the Barguzin microcontinent [24] (Figure 1). The highest protrusions of the asthenosphere are also confined mainly to its boundaries. According to seismic tomography, the mantle structure is formed by cells in which the hottest areas envelop isometric cold blocks [25], which can be interpreted as the penetration of melt or fluid into the cold and rifted lithosphere.

A clear dependence of the localization of alkaline-basalt fields on the depth of the asthenosphere roof has not been established. The diagram constructed from gravimetry data [12, 26] clearly shows that gravitational minima are projected onto the gentle protrusions of the asthenosphere established from seismic data. All volcanic plateaus are confined to roof bends. The protrusions most likely correspond to mantle diapirs [27]. When they rise, the melts that are usually present in the upper part are characterized by slightly higher degrees of melting, and have less viscosity and mobility than water-saturated alkaline melts, which are characteristic of deep levels. The former, most likely, break through into the crust and, due to mixing, form intermediate centers of melting above the roof of mantle diapirs initiated by plume magmas. Due to mixing with the crustal source, basalts in the upper part are inevitably transformed into magmas of medium and acidic composition, which are relatively inactive. Only in rare cases, for example, on the Udokan plateau [11], hybrid magmas of this type penetrate to the surface. More alkaline melts, which appear at the final stages of plume development, can penetrate relatively weakened zones along the periphery of mantle diapirs. They can form ring structures, penetrating along marginal faults that flare the protrusions of mantle diapirs which intrude the base of the Earth's crust proposes options for the formation of ring structures with the conjugate development of magma chambers and mantle diapirs.

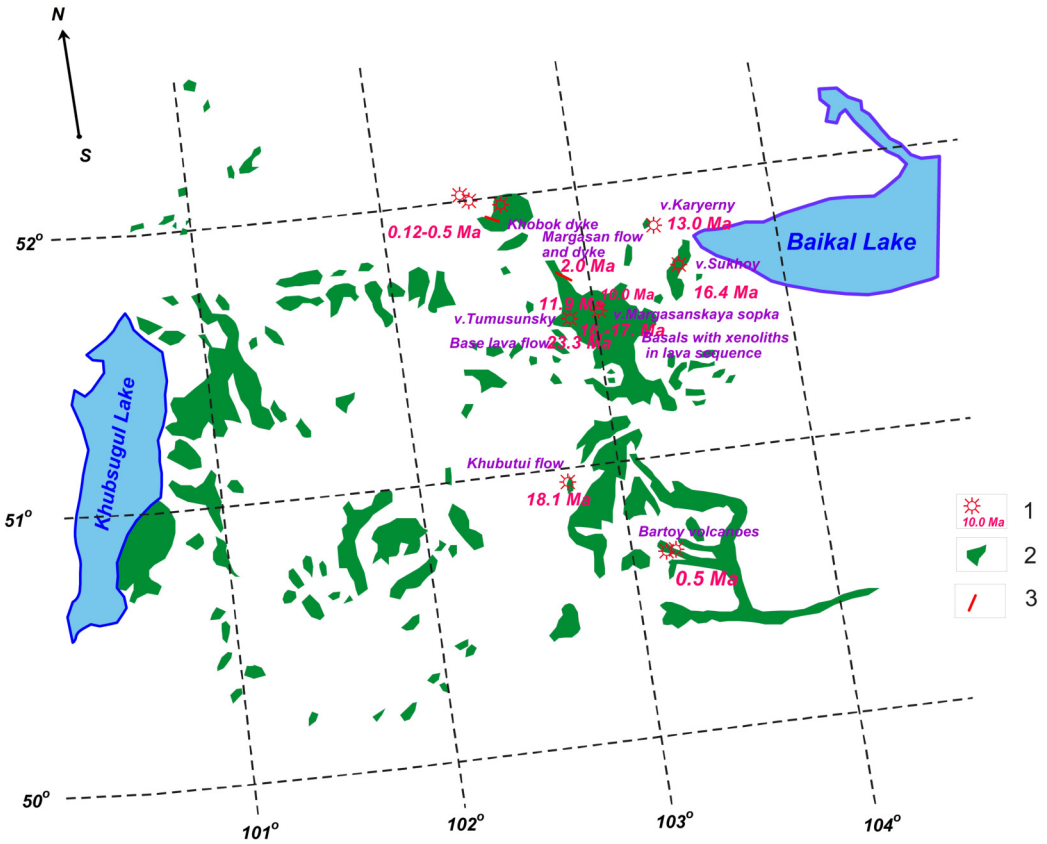

Figure 1. Distribution of the Trans-Khamar-Daban volcanic zone and adjacent areas. The localities are marked by violet stars and their ages in Ma are given in red. (1) Volcanic centers and their ages. (2) Basalt covers. (3) Basaltic dykes.

In this article we give the information about the Trans-Khabar-Daban volcanic zone, which crosses the mountain area 200 km from the Tunka Valley at the north to the Dzhida Valley at the south. This work includes the data concerning the chemistry of the rocks and minerals for host lavas and their crust and mantle xenoliths, the thermobarometry of mantle inclusions and geochemistry of minerals of deep-seated inclusions, and the dating of zircons from granulites as well.

In this paper, we are summarizing the investigations of the Trans-Khabar-Daban volcanic zone which crosses the mountain area 200 km from Tunka valley at the north to Dzhida valley at the south. We are adding new data for the geochemistry of mantle xenoliths and xenocryst to evaluate the chemistry of the rocks and minerals for host lavas and their crust and mantle xenoliths. We show the detail thermobarometry of mantle inclusions using new data including new finding garnet bearing pyroxenites and peridotite inclusions in several localities (Karierny, Margasan) and systematically describe the geochemistry of minerals of deep-seated inclusions, and ages of zircon grains from the granulite to understand the genesis and tectonic significance. Such crosses of TKHVZ were not earlier represented in the scientific literature and high amount of data are completely new.

2. Geology

2.1. Trans-Khamar Daban Volcanic Zone Location

Late Cenozoic plume-related magmatism occurred widespread over Eurasia. The Trans-Khamar Daban volcanic zone (TKDVZ) is the part of the huge area of Central Asia from Tuva in the Sayan Mountains to Primorye covered by Cenozoic flood basalt volcanism. At the western border it contacted the Khubsugul area in Mongolia [28]; in the northwest the continuation is found in Zabit, another area in Eastern Sayan [29], and in the south there are volcanic fields between the Selenga and Orhon rivers. And further, it goes to the Khangai Ridge [30] (Figure 1). The creation of the volcanic TKVZ is the sub-meridional ~200 structure that starts from the Arshan area in Tunka valley [31, 32] and goes to the south through the valleys to the Margasan River to the Tumusunsky and Margasanskaya sopka volcanoes (Figure 2) [15, 33, 34]. Further, this part of the TKVZ continues at the southern slope by Khamney and Tsakirka valley basalts carrying mantle xenoliths. And the southern margin is finished by the Bartoy volcanoes near the Dzhida valley [20, 35, 36].

At the Khamar-Daban xenolith-bearing basalts are known in 5 age intervals. At the base in the center of the plateau, having 400 m in thickness [15] under the Tumusun volcano (23 million years), in the valleys of the Khubutui and Tsakirka rivers (18.1 million years) [13] in the south, and in the Komar ridge [13, 15, 31] covering lava flows and the Sykhoy volcano in the north, there are lherzolite inclusions [15] (Stage I). The host lavas are everywhere in Mg-basanites (Figure 3, sign 1). The pack of lavas under the Tumusunsky volcano is composed of flows of Hy-standard lavas from below, then alkaline basalts (up to 20 m) with megacrystals of anorthoclase. The interbedding of subalkaline and alkaline basalts is completed by the formation of basanites with a variety of cumulative and rare lherzolite inclusions (16–17 million years) (Stage II). The top volcanoes at the center of the ridge and slopes were created at the (Stage III) 13–10 Ma. The post-erosion lava flows were concentrated at the valleys and the slopes (5–2 Ma). The cinder cone volcanoes and associated lava flows developed on the margin of the Khamar-Daban plateau in rift valleys (Stage V) [12, 13, 15, 20, 31, 35, 36] (Figure 2).

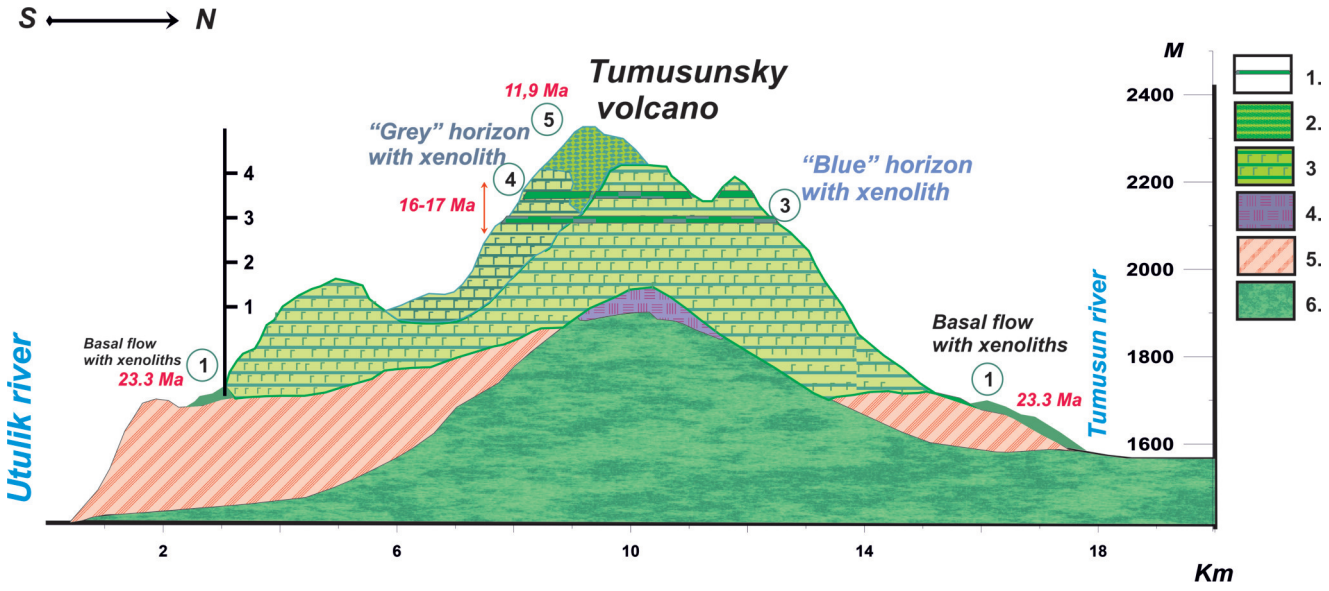

Figure 2. The cross-section of the central part of the Trans-Khamar-Daban zone near Tumusunsky volcano [15]. (1) Horizons with mantle xenoliths. (2) Tumusun volcano extrusive center. (3) Basaltic lava sequence. (4) Volcanic tuffs. (5) Proterozoic gneisses. (6) Slopes covered by vegetation.

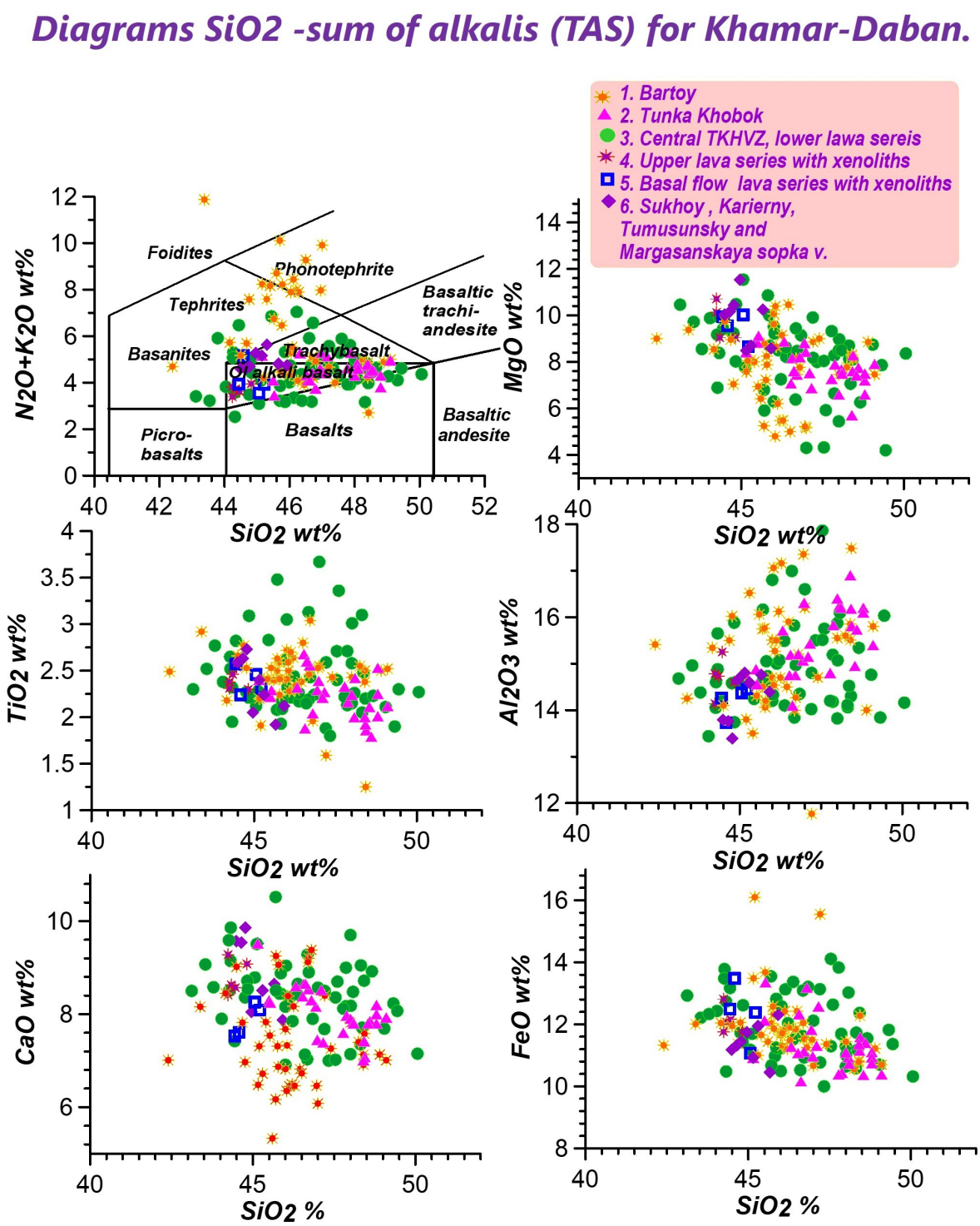

Figure 3. Total alkalis—Silica (TAS) diagram and variation diagram for the composition of lavas from the Trans-Khamar-Daban volcanic zone [15]. (1) Bartoy. (2) Tunka Khobok. (3) Central TKHVZ, lower lava series. (4) Upper lava series with xenoliths. (5) Basal flow lava series with xenoliths. (6) Sukhoy, Karierny, Tumusunsky and Margasanskaya sopka volcanoes.

2.2. Tunka Valley

The ages of the Sykhoy volcano (16.4 million years (Ma) [13, 15] and the Karierny volcanoes at the marginal faults of the rift are about 13 Ma [31, 32]. After them, with a significant break, there are intrusions and tephra deposits from the volcanoes Margasanskaya Sopka and Tumusunsky [13, 15, 33, 34] (11.9–10 million years). The dykes and xenoliths bearing basalt flows in the Khobok River in the Tunka Valley are about 8–9 Ma [13, 15, 31] (III stage). Post-erosion flows (IV) are known on the north-

ern (8 to 2 Ma) [15, 32] and southern (5–2 Ma) slopes of the ridge [13]. Tephra cinder cone volcanoes of 1.5–0.8 million years old with rare mantle xenoliths containing megacrysts of various mega- and xenocrystic pyroxenes, amphiboles (Amph), and phlogopites (Phl), as well as prevailing pyroxenites and crustal xenoliths, are localized in the Tunka valleys at the northern slope of the ridge, mainly to the west from the Elovsky spur covered by the earliest lava sequence [15].

2.3. Dzhida Valley

In Dzhida zone in the southern part of TKDVZ the valleys of Dzhida rivers and their tributaries are covered by the post-erosion basalts sometimes associated with the volcanoes. The basalts have ages 8–5 Ma and the most young Bartoy volcanoes were dated as 0.5 Ma [13, 35, 36].

3. Petrography of Mantle Zenoliths

The petrography of xenoliths Trans-Khamar-Daban zone shows much variation [15, 29–36]. They are relating to both black (Fe–Ti enriched, basaltic derivates) and green (Cr-bearing mantle) types [36]. At the central part of the volcanic ridge of the Tumusunsky and Margasanskaya sopka [15, 35, 36] volcanoes, primitive lherzolitic xenoliths with foliation texture dominate and have orthopyroxene (Opx) (5–10%), clinopyroxene (CPx) (10–20%), olivine (Ol) chromium spinel (Cr–Sp) (1–3%) as major minerals and phlogopites (Phl) (1–3%) s and amphiboles (Amph)(1–2%) as secondary. They sometimes form pink aggregates and symplectites after garnet (Gar). In addition, we found large amount of Sp-Cpx simplectites having rounded outlines after garnet in pyroxenites. Basaltic flows at the base of the volcanic sequence section by the Tumusunsky volcano also contain lherzolitic xenolith slightly more Ol-rich and less foliated. The xenoliths-bearing lava horizons (more silica rich and grey and bluish in color are located in the upper part of the volcanic section (Figure 2). They mostly contain cumulative plagioclase-bearing pyroxenite inclusions compiled by plagioclases (Pl) and Ti-augites in different proportions +Sp. Dark-green colored pyroxenites with spinel are also found there. Granulites represented by Gar-Pl -Amph-Opx and Cpx rocks also occurs.

The location of lavas with the mantle xenolith and pyroxenites inclusions were found in the Margasan river close (30 km) to the Tunka valley near the mouth of the Marta River. Here there is a dyke which contains a large number of green Cr-bearing inclusions -lherzolites and pyroxenites sometimes also containing pink and symplectitic aggregates. There are also black and green (Cr-bearing) pyroxenites with pyrope garnets newly found there. Among the megacrysts there are pyrope almandine garnets, Al–Ti-augites and ilmenites and anorthoclases increased interest in eruption prediction and volcanic hazard mitigation, which also requires monitoring these magmatic systems and understanding the associated fluid migration and deformation processes. To mitigate the impact of volcanic events, it is essential to improve eruption forecasts through innovative observations, advanced methods, and refined models of volcanic processes. Observations through geochemical and geophysical techniques enable the study of volcanic processes across scales, from the microscopic (e.g., magma crystal content) to the macroscopic (e.g., lava flow paths).

In Sukhoy volcano on the Kamar ridge located 12 km south of the of Slyudyanka [15, 32] there are Sp-lherzolites, and various black pyroxenites essentially Ti-augitic. At the southern slope of Khamar-Daban lherzolite xenoliths and Ti-augite megacrysts were found in the lava flows covering valley of Khamney and Tsakirka Rivers. In the Tunka valley near the Arshan resort on the Khobok River, various inclusions of both black and green types [15] have been described [12], and both spinels and plagioclase- bearing pyroxenites prevail, chromium lherzolite are extremely rare among xenoliths found mainly in volcanoes that surround the Arshan from the south. A large number of deep-seated inclusions were selected at the quarry of Karierny volcano 30 km to the west of Lake Baikal. Th light-green dry lherzolites are abundant in this locality [33]. In addition, a variety of pyroxenite has been found. Some Cr-bearing pyroxenites contain garnet together with spinel. The black pyroxenites show high variations in composition petrography and texture. Some garnet granulites were also found in this location.

Very diverse inclusion set is found in lavas and tuffs of Bartoy volcanoes [15, 20, 35, 36]. The spinel lherzolites often contain mica and amphiboles. The diverse pyroxenites of Cr—types with spinels and sometimes hydrous phases and of black types are also widespread. In the megacrystic set there are Ti–Al augites, almandine-pyropes, kaersutitic amphiboles Ti-biotites, alkaline feldspars, Ti magnetites and ilmenites, corunds, rutiles and rare zircons also occur. The megacrystic phases are often in intergrowths up to 10 cm in diameter. There are complex nodules presented the contacts of various petrographic groups. The granulite xenoliths with and without garnets are also diverse.

In the Sukhoy volcano on the Kamar ridge, located 12 km south of Slyudyanka [15, 32], there are Sp-lherzolites and green (Cr-bearing) pyroxenites with garnets and various black pyroxenites with garnet plagioclase and spinels have been discovered there. Contacts between lherzolites and pyroxenites are observed very often.

At the southern slope of Khamar-Daban, lherzolite xenoliths and Ti-augite megacrysts were found in the lava flows covering the valley of the Khamney and Tsakirka Rivers.

In the Tunka valley near the Arshan resort on the Khobok River, various inclusions of both black and green types [15, 32] have been described, and both spinel- and plagioclase-bearing pyroxenites prevail. The lherzolites with the Cr-diopsides are extremely rare among xenoliths and were found mainly in volcanoes that surround the Arshan from the south and in Khobok volcano.

A huge number of deep-seated inclusions were selected at the quarry of Karierny volcano 30 km to the west

of Lake Baikal. The light-green lherzolites sometimes with amphiboles and micas are abundant there [12, 33]. In addition, a variety of pyroxenites has been found. Some Cr-bearing pyroxenites contain garnet (new finding for this article) but mostly spinel. The black pyroxenites show high variations in composition, petrography, and texture. The garnet granulites were also found.

A very diverse inclusion set is found in lavas and tuffs of Bartoy volcanoes [15, 20, 35, 36]. The spinels lherzolites often contain mica and amphiboles. The diverse pyroxenites of Cr-types with spinels and sometimes hydrous phases and of black types are also widespread. In the megacrystic set there are Ti–Al augites, almandine-pyropes, and kaersutitic amphiboles. Ti-biotites, alkaline feldspars, Ti-magnetites and ilmenites, and rare zircons also occur. The megacrystic phases are often in intergrowths up to 10 cm in diameter. There are complex nodules presented in the contacts of various petrographic groups. The granulite xenoliths with and without garnets are also diverse.

In TKBVZ fresh pyrope garnets were not found in the lherzolites like in was found in Vitim [14, 15]. Khentei [30] and Eastern Sayan [29, 37] but we found them in Cr-pyroxenites of Karierny and Margasan river dyke and the first mention is in this artickle.

4. Methods of Investigations

4.1. Electron Probe Microanalysis

The minerals from xenoliths were put in epoxy mounts and also the polished thin sections were prepared. They were analyzed in the Analytic Center of IGM SM RAS using electron microprobe analysis (EPMA). It was performed using Camebax Micro and Jeol JXA8320 apparatus according to the published procedure [38]. The sizes of the electron beam were 1 µm. The accelerating voltage was 15 kV, and the beam current was 15 or 20 nA with 15 s counting time. The relative standard deviation did not exceed 1.5%; the precision was close to 3–5% 2 sigma error.

4.2. Scanning Electron Microscopy

In addition minerals in thin sections were analyzed using a MIRA 3 LMU scanning electron microscope with an attached INCA Energy 450 XMax 80 microanalysis energy-dispersive system (SEM-EDS) at the X-ray Laboratory of the Institute of Geology and Mineralogy, Siberian Branch, Russian Academy of Sciences (analysts Ashchepkov I.V., Karmanov N.S.). See Supplementary File S2.

4.3. X–Ray Fluorescence Silicate Analysis

The bulk rock analyses of the rock powder were obtained by X-ray fluorescence silicate analysis of rocks for major components—Na_2O, MgO, Al_2O_3, SiO_2, P_2O_5, K_2O, CaO, TiO_2, V_2O_5, Cr_2O_3, MnO, Fe_2O_3, NiO, BaO, and volatile losses—and were used to estimate bulk rock compositions of basalts and xenoliths. They were analyzed in the Laboratory of X-ray Spectral Methods of Analysis IGM SB RAS using an X-ray fluorescence spectrometer ARL 9900XP (Thermo Fisher Scientific) with sample preparation equipment: a KATANAX X-300 electrothermal three-position furnace and a HERZOG HTP-40 press. The results satisfy the third accuracy class with lower limits of the determined contents of 0.1–0.00n. The analyses are in the Supplementary File S2.

4.4. Inductively Coupled Mass Spectrometry with Laser Ablation (LA ICP MS)

Mineral grains of clinopyroxenes, orthopyroxenes, amphiboles, garnets, feldspars, olivines, phlogopites and biotites, and amphiboles from the concentrate of grains from xenoliths of TKVZ (70 grains) were analyzed by laser ablation inductively coupled plasma mass spectrometry (LA-ICP-MS) in the Institute of Geology and Mineralogy SB RAS using an iCAP Q mass spectrometer (Thermo Scientific, Waltham, MA, USA) and an NWR 213 (New Wave Research), Nd YAG:UV 133 nm laser ablation system (analyst N.S. Medvedev). The method has a detection limit of $\sim 10^{-7}$, and the standard deviation of the measurements for most isotopes was about 10–25%. In total, 54 isotopes of elements were analyzed. The NIST 612 and 610 SRMs were used as the standards. For the internal control, 24Mg, 29Si, 39K, 47Ti, 55Mn, 52Cr, 40Ca, 27Al, and 23Na isotopes were used to check agreement with EPMA analyses and to estimate the trace element level. The 40Ca isotope was used for the normalization of the initial values. Additionally, garnets and clinopyroxenes from samples 315–254, 315–167, and 315–73 were analyzed in MRAC Belgium by solution ICP-MS [39] and were used as internal standards. In addition, we used the LA ICP MS analyses of mineral grains from xenoliths of TKVZ made previously using the Element II mass spectrometer. The analyses are in Supplementary File S3.

4.5. Isotopic Dating using LA ICP-MS of Zircons from Xenoliths and Concentrates from Volcanic Tuffs

The detailed mineral compositions of (>900) grains in or the dating of the same inductively coupled mass spectrometry with laser ablation aniCAP Q mass spectrometer (Thermo Scientific) and an NWR 213 (New Wave Research) were used. For dating, isotopes 235U, 238U, 207Pb, and 205Pb, and in addition 206U, 208U, 232Th, 171Zr, and 177Hf were analyzed. The time for measurements of each sample was 90 s. Isotopic ratios of 207Pb/235U and 206Pb/238U after the subtraction of blanks were used for the age calculations, projecting them on the Concordia line. As the standards, the Plešovice [40], SA-01 [41], and Mud tank [42] were used as well as NIST610. The age was determined using the Isoplote3 program [43]. See Supplementary File S4.

5. Bulk rock Compositions of Volcanic Rocks and Ages

All basaltic lava series in TKVZ were dated by K–Ar and Ar–Ar methods and divided into 5 age intervals [13]. In the center of the plateau (Figure 2), under the Tumusun volcano, the xenolith-bearing Ol-alkali basalts are found at the base of the 400 m thick lava flow [15] at the south and north from the volcano were dated 23 Ma. Tephra coats from the volcanoes Margasanskaya Sopka and Tumusunsky (10–11.9 million years old) [13] lie on them with a significant break. In the north, in the Sykhoy (16 Ma) volcano, the Komarsky cover is in the north, and in the Karierny volcano (15–13 Ma), Mg-sub-alkali basalts contain lherzolite inclusions (Figure 3). Total Alkalis-Silica (TAS) diagram and variation diagram for the composition of lavas from the Trans-Khamar-Daban volcanic zone everywhere (III stage). Post-erosion flows (IV) are known on the northern part (Margasan River) (from 8 to 2 million years old) [13, 15], and the southern slopes of the Khabar-Daban ridge lava flows and dykes mainly trace river valleys (5–2 million years old). Abundant latest cinder cone volcanoes and accompanied dykes and flows of various alkaline basalts, basanites, hawaiites (tephrites), and mujeirites (phonotephrites) (0.12–0.8 million years old) with diverse xenoliths are localized in the Tunka and Dzhida valleys (with Amph and Phl) on the northern and southern parts of the basaltic plateau, respectively (V stage). The most varying in composition of lavas are occurring in Bartoy volcanoes. Variations of the lava compositions of the Khamar-Daban volcanic zone are shown in the diagram (Figure 3). In general, there are continuous variations of lavas in other regions of the Baikal Rift zone [11–13, 15, 21, 31, 32, 37]. See Supplementary File S1.

6. Bulk Rock Compositions of Mantle and Crust Xenoliths

6.1. Variations of Xenolith Bulk Rock Compositions from TKVZ

The variations of the xenolith bulk rock compositions from TKVZ presented in the diagram (Figure 4) show a rather restricted range of the common spinel peridotites prevailing in TKVZ. They show the SiO_2 range from 41 to 46, extending to 47 wt% for reactional association, showing a small increase in CaO to 7 wt%, Al_2O_3 to 8 wt%, alkalis Na_2O to 1.5 wt%, and TiO_2 to 0.7 wt% with FeO to 11 wt%. The other rocks may be divided into cumulates from mostly basaltic melts and crustal xenoliths divided by the inclined lines at ~48 SiO_2 wt% (Figure 4A).

6.2. Variations of Xenolith Bulk Rock Compositions from Bartoy Volcanoes

Bartoy xenolith bulk rock variations are presented in the next diagram (Figure 4B). The lherzolites were subdivided into groups according to indicator minerals—Amph-bearing, Amph-Phl-bearing, Phl—bearing and dry types. The dry group are at the center 44–46 SiO_2 wt%. The Amph-Phl are also at the center but are slightly higher in alkalis and TiO_2. The Phl-bearing are a bit more FeO and SiO_2, K_2O enriched. Pyroxenites are essentially higher in CaO and Al_2O_3 and TiO_2 and highly varying in SiO_2. The crustal xenoliths contain more than 50 wt% SiO_2.

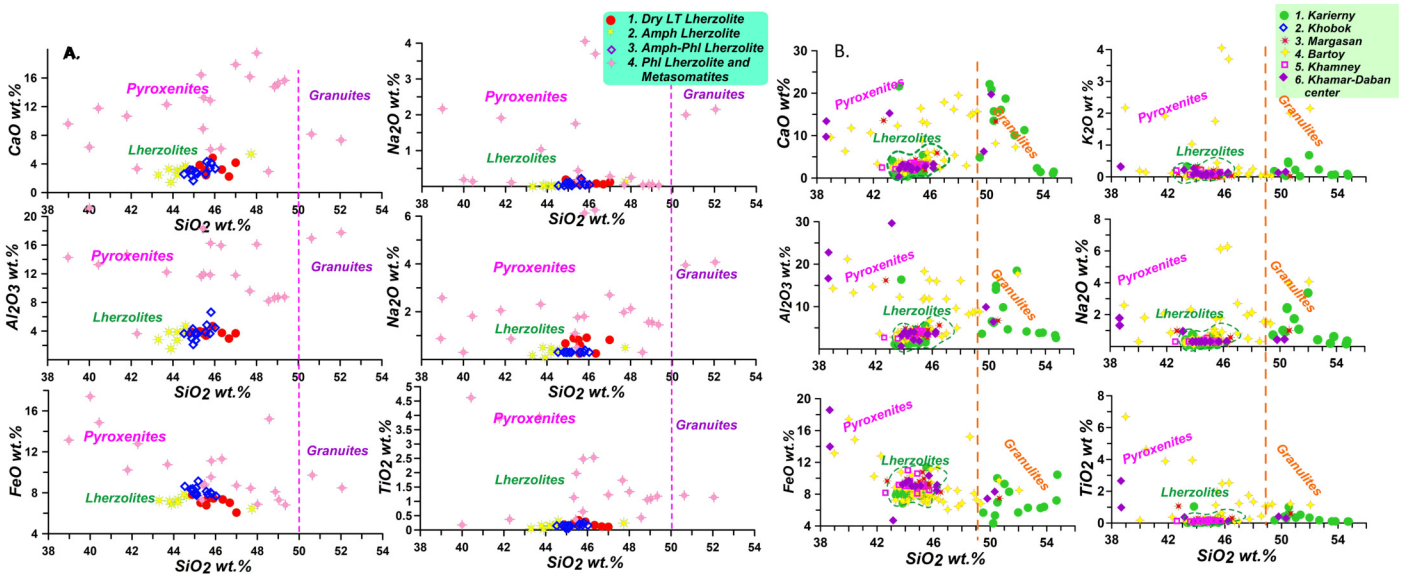

Figure 4. Bulk rock composition of xenolith from: (**A**) Trans-Khamar-Daban volcanic zone: (1) Karierny. (2) Khobok. (3) Margasan. (4) Bartoy. (5) Khamney. (6) Khamar-Daban center. (**B**) Bartoy volcanoes. (1) Dry Low temperature Lherzolite. (2) Amph Lherzolite. (3) Amph-Phl Lherzolite. (4) Phl Lherzolite and Metasomatites.

7. Mineral Chemistry of Mantle and Crustal Xenoliths

7.1. Clinopyroxenes

The Cpx from xenolith are separated into the four major large groups in the diagrams. The typical mantle xenoliths (group 1) are forming the trend from 1.5 to 3.5 wt% FeO (Figure 5), which is accompanied by the growth of Al_2O_3 to 9 wt%, Na_2O to 3 wt%, and TiO_2 to 2.5 wt% and the decrease of Cr_2O_3 from 1.75 to 0. For the mantle metasomatites (group 2), FeO is extending to 5.75 wt%. The clinopyroxenes show slightly lower content of minor components than those from group 1 (Figures 5 and 6).

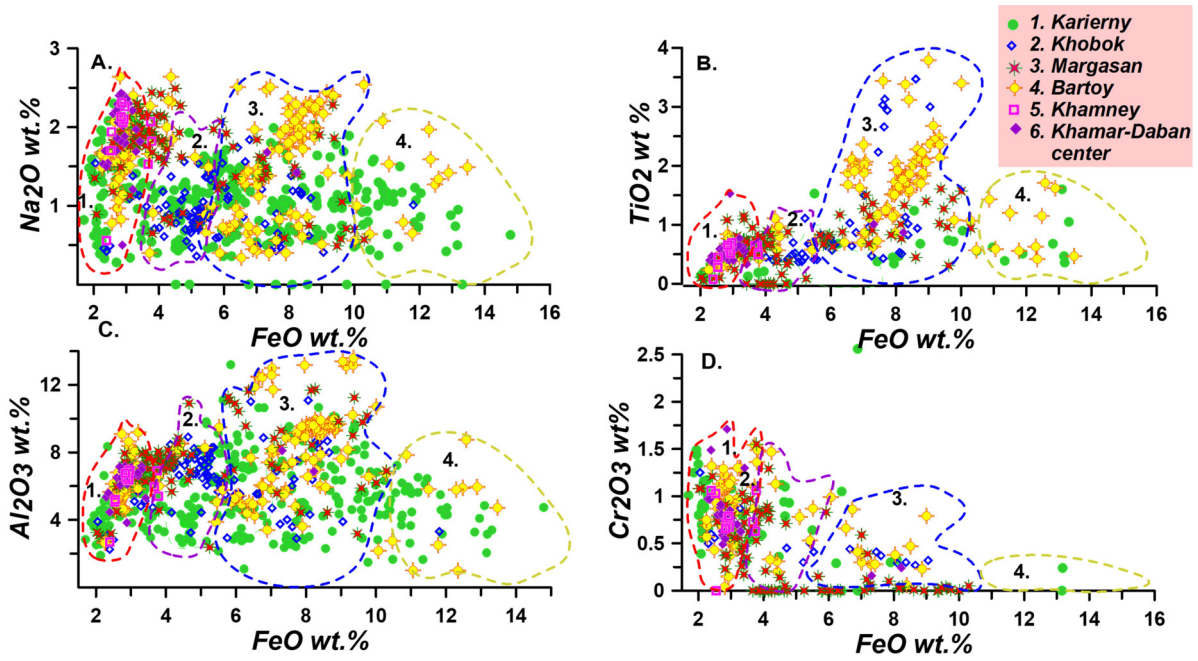

Figure 5. Variation diagram for the clinopyroxenes from TKVZ. (1) Karierny. (2) Khobok. (3) Margasan. (4) Bartoy. (5) Khamney. (6) Khamar-Daban center.

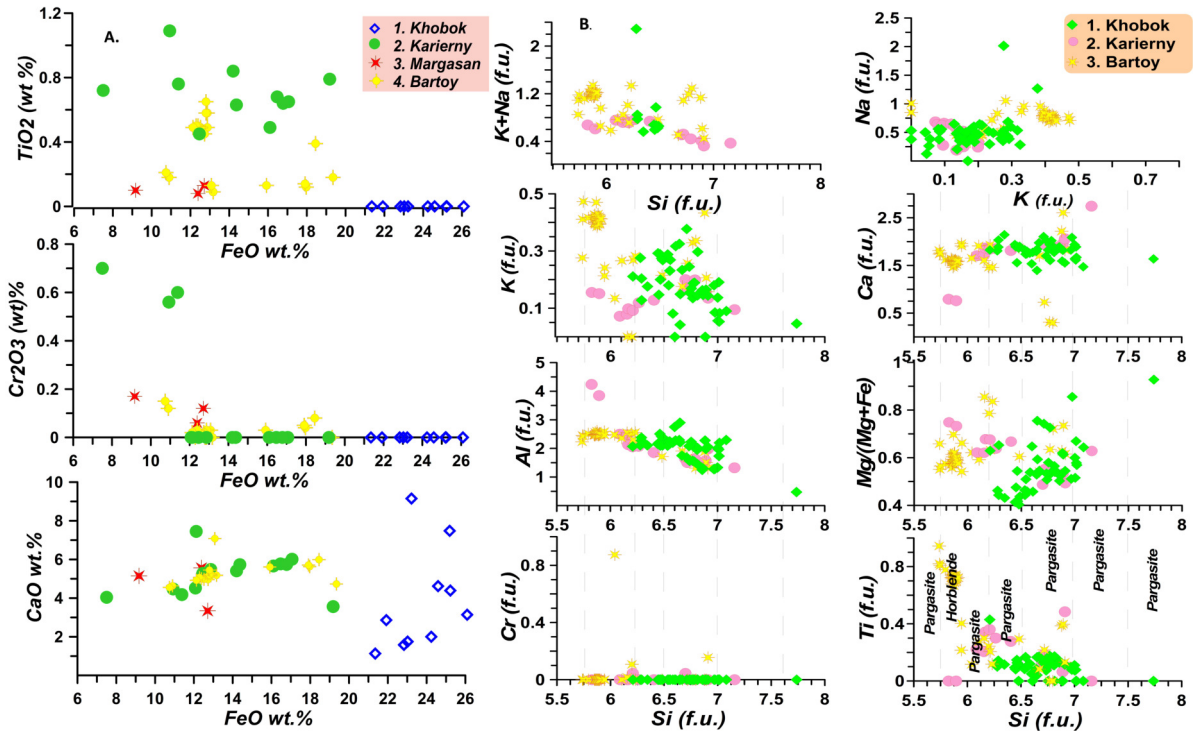

Figure 6. Variation diagrams for: (**A**) Garnets: (1) Khobok. (2) Karierny. (3) Margasan. (4) Bartoy. (**B**) Amphiboles: (1) Khobok. (2) Karierny. (3) Bartoy.

7.2. Garnets

Garnets are also represented by the transitional varieties, 1–2 grains in each locality. They show up to 0.7–1.3 wt%. Cr_2O_3 is in the Karierny volcano and much lower in the Bartoy and Margasan localities, while TiO_2 varies from 0.15 to 0.3 wt% and CaO from 4 to 5 wt% (Figure 7A). In megacrysts the TiO_2 is rather high—0.9–0.6 wt%—and the Cr_2O_3 is low, 0–0.2 wt%. Pyroxenites and granulites display highly varying CaO (1–10 wt%) and an absence of Cr_2O_3 and TiO_2.

Group 3 mantle megacrysts and pyroxenites demonstrate very high growth of Al_2O_3 to 14 wt%, TiO_2 to 4 wt%, and Na_2O to 3 wt% near 9 wt% FeO but a decrease of Cr_2O_3 to 1 wt% or less. The crustal pyroxenites and granulites vary highly in SiO_2. The crustal xenoliths contain more than 50 wt% SiO_2 (group 4) with FeO >10 wt% shows a general smooth decrease of the same components (TiO_2, Al_2O_3, Na_2O) during FeO growth from 10 to 16 wt%. The highest variations reveal the Cpx from Bartoy and slightly fewer samples from the Karierny volcanoes. Those from Margasan reveal similar fluctuations within the first 2 groups but are less megacrystic. Clinopyroxenes from Khobok volcano mainly represent 2 groups. And two sites from the Center of Khamar-Daban display only lherzolitic clinopyroxene variations.

7.3. Orthopyroxenes

The variations of Opx in general represent mainly variations of the lherzolitic compositions from 4 to 8 wt% FeO They have 1–18 wt% Cr_2O_3 and Al_2O_3 to 9 wt% and to 1.1 wt% TiO_2 decreasing with FeO growth. The reactional orthopyroxenes (8–11 wt% FeO) show 0.8 wt% TiO_2 and 0.9 Ti, and the Cr_2O_3 megacrystic suites reveal 11–16.8 wt% FeO, 0.35–0.15 Cr_2O_3, and 0.7–0.5 wt% TiO_2. The pyroxenitic varieties are much lower in Cr_2O_3 and sometimes are high in TiO_2 to 0.8 wt%. All complete groups are represented in xenoliths from the Bartoy and Karierny volcanoes also, but they are much lower in all admixtures; the Margasan xenoliths are represented by one transitional garnet and two megacrystic grains.

7.4. Amphiboles

Amphiboles from xenoliths from the Bartoy and Karierny volcanoes display similar variations, but those from Bartoy are more variable. The xenoliths of lower crust granulites contain quite various amphiboles. The subdivision of amphiboles was made according to published nomenclature [44]. The main trend starts from the typical hornblendes to edenites with the decrease of Al from 3 to 1 formula units (f.u.); the deviations to the higher Al values are found for several amphiboles, mainly from the Vitim xenolith (Figure 7B). The continuation with the higher Si values was determined for several K–Na richterites from Vitim and some actinolites from Tunka. This range is accompanied by the essential decrease of the Ti, highest for the hornblendes frequent in Bartoy (up to 1 formula unit) and rapidly decreasing for pargasites and other varieties. Mg is varying and is splitting with the Si rise according to deviations to alkaline and Ca branches. The Ca content is nearly constant to edenites and then rapidly decreases. The alkalis (Na+K) are decreasing together with the Al content and silica growth, though there are some deviations.

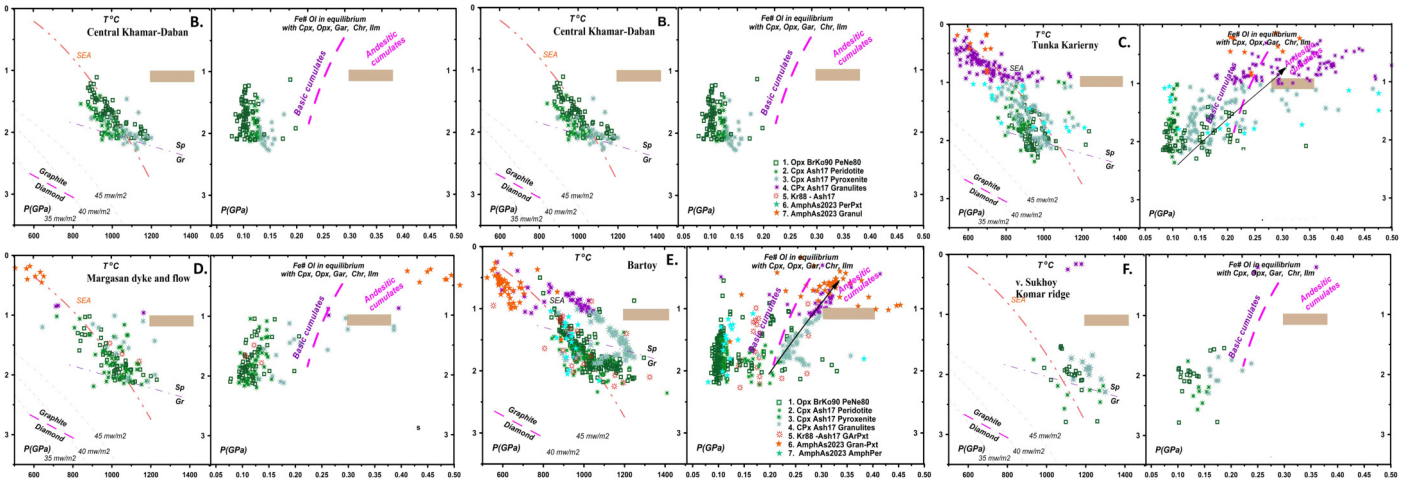

Figure 7. PTX diagram for the xenoliths and xenocrysts of volcanic rocks from TKDVZ. Signs: (1) Opx: T °C [45]- P (GPa) [46]. (2) Clinopyroxene: Peridotites: T °C- [47], - P (GPa) [48]; (3) Clinopyroxene: Pyroxenite: T °C [47], P (GPa) [48] for pyroxenites. (4) The same for granulites; (5) Garnet (monomineral) T °C [49] - P (GPa) [48], (6) Amphibole: T °C [50] P (GPa) [51]; (7) The same for granulites. (**A**) Khobok Dyke and volcano; (**B**) Karierny volcano; (**C**) Sukhoy volcano; (**D**) Central Khamar-Daban; (**E**) Margasan flow and dyke; (**F**) Bartoy volcanoes The horizontal dashed line at 3.5 and 4.5 GPa corresponds to the Graphite-Diamond boundary at 35 and 40 mW m^2 respectively. Conductive geotherms after [52].

8. Thermobarometric Reconstructions

8.1. Tunka Valley and Kamar Ridge

Khobok volcano in the Tunka valley near the Arshan resort is one of several small cinder cone volcanoes with xenoliths. The most abundant in xenoliths locality dyke is located on the Khobok riverbank near the Kovrizhka volcano [15, 31]. Rare green Cr-diopsides from xenolith give 1.7–1.1 GPa and a location about 100–150 °C below the South East Australia Geotherm (SEA) geotherm [53]; only one gives a very high-temperature (HT) ∼1300 °C position. The black, commonly Sp-Mgt-bearing clinopyroxenes give the pressures from 1.8 to 1.0 GPa and highly varying temperatures, locating near the SEA geotherm at the higher depth and variations from 700 to 1200 °C near and at the Mono boundary. The black pyroxenites just above the Moho at 10–7.5 GPa also show variations from 650 to 1100 °C. Further above 0.7 GPa are located the estimates for the amphiboles from amphibolites; they are grouped near the SEA. In P–Fe#, the lherzolitic minerals are grouped near 0.1 Fe#. The megacrystic-pyroxenitic range rises from 0.12 to 0.3, and the cumulates in and above the Moho vary from 0.15 to 0.35, while the amphibolites go to 0.6 and more (Figure 7A).

Karierny volcano. The PT conditions in the PTX diagram for the Karierny volcano [12, 32] in the eastern part of the Tunka valley show the pressure range from 2.2 GPa to Moho. The enstatite-Cr-diopside branch trace SEA geotherm and lowering up to ∼170 °C at 1.7–2.0 GPa. The heating at the mantle base is very high, up to 1250 °C (Figure 7B). And even at the upper boundary of the Moho, the Fe-rich pyroxenites (granulites) are heated to 1200 °C. The estimates for the Cr-bearing hornblendes and pargasites are tracing the Cr-diopside branch from 1.7 GPa to Moho; the PT for kaersutites and pargasites from pyroxenites duplicate the estimates for Ti-augites. In crust conditions starting from 0.8 GPa are the pyroxene and amphibole estimates. There are two PT estimates for the Ct-bearing garnets from pyroxenites showing variations from 1.4 to 1.9 GPa plotting on the lower temperature geotherm. They are plotting above the Gar-Sp transition, but this boundary is for the lherzolitic compositions, but these samples are Cr-pyroxenitic. The megacrystic trend for CPx shows a rise of Fe# from 0.15 to 0.25 when reaching the Moho and then rises to 0.5 Fe# trace common SEA plum geotherm and becoming lower with pressure (Figure 7B). The megacrystic trend for CPx show rise of Fe# from 0.15 to 0.25 when reaching Moho and then are rising to 0.5 Fe#.

Sukhoy volcano. The Cr-bearing lherzolitic minerals with high Fe# are very high temperature and represent the contact associating s giving up to 1350 °C locating far above the SEA geotherm. But common Cr-diopsides trace the low temperature branch from 1.7 GPa to 1.5 GPa (Figure 7C).

8.2. Central Part of Khamar-Daban Ridge

Tumusun volcano. In the central part of the ridge in the Tumusun volcano, the lherzolitic inclusions trace exactly SEA according to the orthopyroxene [46] from 1.9 to 1.4 GPa. The clinopyroxene PT estimates reveal more scattering (Figure 7D).

Khubutui lava flow. The xenolith from this location demonstrates nearly the same PT plot (slightly lower in pressure) as the lherzolitic xenoliths from the southern part of TKVZ.

The Margasan lava flow and dyke from the Margasan River near it in the northern part of the Khabar-Daban range give a more continuous TP range from 2.3 GPa to Moho, showing the division into three clots and continuous Fe# growth of 0.07–0.13. The megacrystic PT reveals a sub-adiabatic trend of 1230 °C from the base to the Moho and Fe# growth of 0.15–0.2. The pyroxenites above the Moho reveal higher Fe# variations (Figure 7E).

8.3. Dzhida Valley

Bartoy volcanic group. The mantle material is more regularly heated, and enstatites and Cr-diopsides, together with the Cr-hornblendes and rare pyroxenitic garnets, just follow SEA geotherm. There is a subparallel lherzolitic trend with the temperatures about 50–100 °C or lower. The lherzolitic PT estimates traced by both pyroxenes are also followed by the PT points of Cr-bearing amphiboles and garnets from the reactional peridotites formed at the contacts (Figure 7F). At the base of the mantle column (∼2.0 GPa), the geotherm shows the vast heating range from 1350 to 900 °C, reflecting the interaction of the basaltic melts with the peridotites. The pyroxenitic branch starts at 1250 °C and goes to 950 °C at the Moho boundary and is even introduced into the crust to 0.5 GPa. It is also traced by the PT points for the pyrope and kaersutite megacrysts. The pyroxenitic PT estimates at the Moho show a range from high temperatures to ∼650 °C. The PT points for the crust amphiboles are mostly lower in temperature than SEAG, but there are spots continuing the megacrystic geotherm.

The P–Fe# plot shows the separate subvertical line for lherzolites and 0.09–0.11 Fe# for enstatites, Cr-diopsides, and Cr-amphiboles. The rather wide range of 0.09–1.6 GPa from the base of the mantle column reflects interaction with basalts at the base; it is poly-mineral, and the upper part is represented by garnets, amphiboles, and orthopyroxenes. The trend of the megacryst melts differentiation of 0.2–0.35 Fe# from BMC to Moho is represented by Cpx, Opx, and Gar. The high-pressure range at BMC to 0.4 Fe# is formed in the crystallization in the lower chamber.

9. Geochemistry of Minerals

9.1. Karierny Volcano

The clinopyroxenes from peridotites from this site [32] analyzed in this paper show a bit different patterns of trace elements than presented earlier [12, 33]. Two clinopyroxenes from typical spinel lherzolites reveal the flattened REE pattern of ∼10/PM (primitive mantle, according to [54] (Figure 8A, open squares), slightly concave or con-

vex in the LREE part. They show small minima in Zr–Hf and one deep minimum in Ta–Nb in the multicomponent trace element spider diagram (MSD). The others display flattened REE from Lu to Sm and small minima in Eu and elevated left part to (15–120)/PM part. They show nearly the same left part of MSD with minima in Ta–Nb; only one shows a Zr peak and another one in Sr. But most of them show high peaks in Th–U (U is higher), which is typical for carbonatitic metasomatism [55]. These patterns are similar to those from the work of Ailow [32], but ours are more flattened. There are three samples with the inclined HREE part to Lu/PM at 0.7 and 1.6 (open rhombs), similar to REE patterns from garnet lherzolites and MSD-like spinel lherzolites. One amphibole reveals nearly the same elevation in LREE to the 16/PM pattern, but in MSD all the left parts, including large ion lithophile elements (LILE), are higher at (14–15)/PM without minima in Ta–Nb.

9.2. Margasan Lava Flow

The clinopyroxenes from spinel lherzolites of Margasan lava flow show the flattened and slightly concaved REE diagrams slightly above 10/PM. On MSD they have also flattened right part to Ta ab minima in U peaks in U and lowered left part. Two of clinopyroxenes display the LREE depleted starting from Sm diagrams. At the MSD they have also lowered jugged left parts (Figure 8B). One of the Opx show concaved patterns with La at 1.3/PM and Lu ∼11/PM with the peak in Eu. At MSD they also show concaved to U distribution and peaks in Th and Rb. The other Opx reveal coinciding from Lu to Tb patterns and further depleted to Ce but elevated La-diagram. At the MSD it has lowered left part fluctuated near 1/Pm a relative peak in Nb. All minerals have strong peaks in Pb ∼ above 10–15/PM.

9.3. Tumusunsky Volcano

Four clinopyroxenes from the Tumusun volcano also show flattened REE patterns at 10/PM and depleted in LREE from Sm except for one sample at the MSD they also flat distribution till Ta and then one has peak in Nb the others show Th–U peaks.

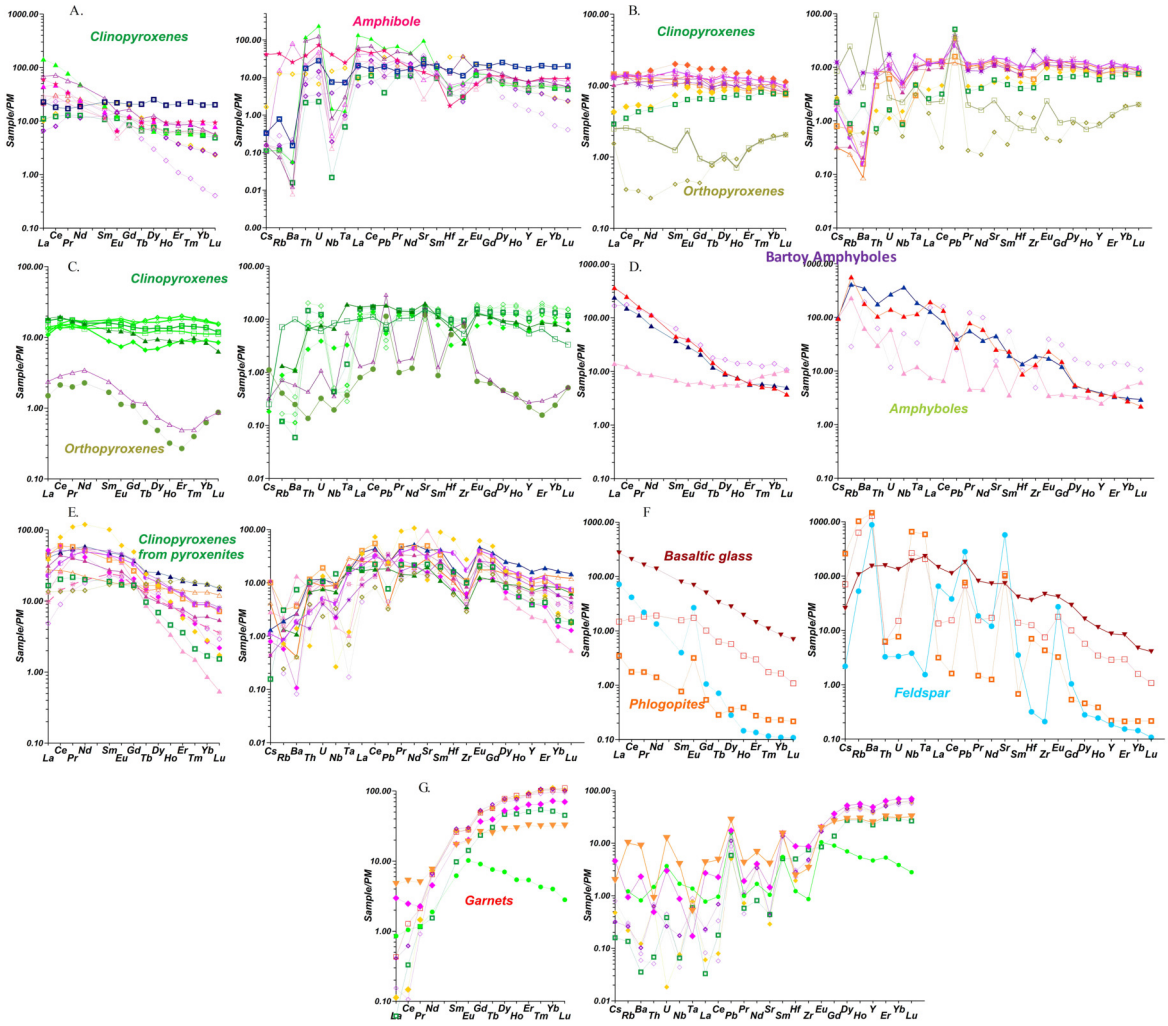

Figure 8. REE and TRE spider diagrams for the minerals from xenoliths from: (**A**) Karierny volcano. (**B**) Margasan dyke and flow. Bartoy volcanoes: (**C**) lherzolites; (**D**) amphiboles; (**E**) pyroxenites and megacrysts; (**F**) micas, feldspars basaltic glass; (**G**) garnets. Normalization to [52].

For the bulk rock compositions [33] they reveal similar flattened distributions but near 1/PM and at the MSD they reveal flattened distributions.

9.4. Bartoy Volcanoes

The lherzolitic Cpx from Bartoy volcanoes have nearly flat REE patterns at 10–12/PM, and one of them has a slightly convex MREE with a small peak in Eu (Figure 8C). But at the MSD they differ. Most of them show minima in HFSE and low LILE but elevated Th–U and Sr. One sample has a completely flat pattern. And those with concave REE display a gradual decrease of left apart and small minima in Zr–Hf. The orthopyroxenes show S-type REE distributions with the peak in Nd at 0.3/PM. He MSD shows strong peaks in Sr, Pb, and Zr–Hf and smaller ones in Th, U, and Nb.

The Cpx from common black pyroxenites display rounded La to Nd and inclined Pr_n (50–70) to Lun (12-3) patterns with the spreading HREE. In MSD, they reveal minima in Ta–Nb and fewer in Hf-Zr and Ba peaks (Figure 8D). The megacrystic (megapyroxenitic) minerals of the Bartoy volcanoes have their individual characteristics. REE patterns of the Ti augites are similar in shape to those from Vitim [12, 14], showing asymmetric bell-like REE patterns with slightly elevated humps with peaks in Sm. But in MSD they reveal minima in Zr $\ll$ Hf but Ta–Nb peaks and again depressions in Th–U and strong peaks in Ba. The Cr-bearing hydridic pyroxenites also display asymmetric bell-like patterns but with the flattened hump from Ce to Sm, ~15–12 at peaks. At the MSD they show deep minima in Ta–Nb. And LILE is smaller in Zr–Hf. But they have elevated U-Th ratio.

The kaersutite reveals a more LREE-enriched, nearly lineal REE pattern with Lan at 80/PM. It shows a similar MSD pattern as clinopyroxene but with depression in Ta–Nb. The Ol megacrysts also reveal a similar humped REE pattern with the top at Sm_n (5/PM) and the very low left part of the MSD. The REE of another kaersutitic amphibole inclined slightly concave in MHREE patterns with La/Sm at 150–120 and Lu at 12–14; in MSD they display elevated LILE up to 140–170 for Rb and are also high in Ta–Nb–Th–U and fluctuated Pb and Zr–Hf. One parasitic amphibole shows the flattened slightly concave patterns ~(12–10)/PM, and in MSD it shows Rb ~ 120 and also peaks in U, Pb, Sr, Zr, and Hf (Figure 8E).

The alkali anorthoclase feldspar shows a highly inclined concave HMREE pattern from La/PM ~ 100 to Lu/PM ~ 0.1 with a high Eu peak. The MSD shows Ba-Rb-Sr and Au peaks and low HFSE. One Ti-biotite show inclined rising from Lu to Al ~ 12/PM REE pattern. The phlogopite displays very low La/PM (~1.2) and Lu/PM (~−0.1) concave REE patterns. And in MSD they show high LILE (~1000/PM) and Nb–Ta and Sr peaks but minima in Th–U. Basaltic glass displays an inclined REE straight-line pattern with La/Yb_n ~ 10. And a gentle convex MSD pattern (Figure 8F).

The garnets of the almandine-pyrope type from the megacrystic group reveal very high HREE (100–70)/PM and a gradual lowering of REE to La/PM ~ 0.08–0.13) with the small inflection in Eu. At the MSD they show fluctuated left parts with elevated U-Nb and lowered LILE. The garnets from hybrid pyroxenites show flat or even rising Pr–Ce–La ~(3–6)/PM. One garnet shows even rising from Lu to Eu and then abrupt lowering to La. In the MSD, the show low HFSE and LILE (Figure 8G).

10. Results of U-Pb Isotopic Dating of Zircons

We obtained the ages of the 6 zircon grains from the tuffs of the Bartoy volcano. They are plotting practically on the207Pb/235U and 206Pb/238U concordia line (Figure 9). They may be divided in to three groups. One near 300 Ma is close to many ages of granites in the TransBaikalia [56–64]. The ages near 810–865 Ma are determined for the suit from the metamorphic in Central Khamar-Daban [64]. The more ancient ages 1070–1265 Ma are definitely belonged to the granulitic xenoliths, though there are granitoid plutons of similar ages [65] (Figure 9). For the calculations ages the polynomial equations were used (see Supplementary File S4).

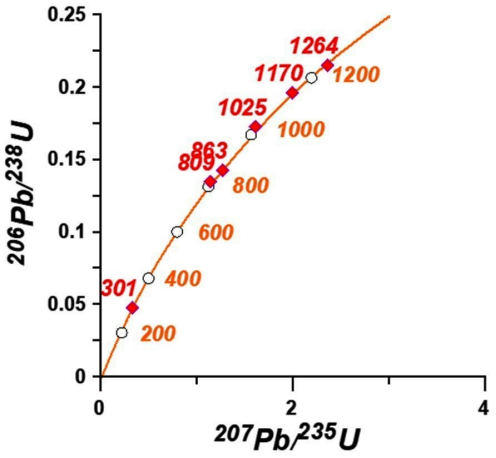

Figure 9. Concordia $^{207}Pb/^{235}U$–$^{206}Pb/^{238}U$ diagram and results of the dating of zircon grains found in tuffs of Bartoy volcanoes.

11. Discussion

11.1. Temporal and Lateral Variations of Xenoliths in TKVZ

Geophysical and tectonic studies indicate the asymmetrical structure of the Baikal rift zone [66–70]. In the northern part, from the Tunka depression, in the Eastern Sayan mountains, the lithospheric thickness reaches more than 250 km [71]. In the center of the Tunka Valley rift, the thin crust is no more than 20 km. Further to the south, the lithospheric thickness is gradually increasing from Khamar-Daban to 50 km or more.

According to the assumptions of many researchers, the plume (hot spot) [19, 27, 29, 32] and accompanied mantle diapir have intruded beneath the Khamar-Daban ridge and adjacent areas. It penetrated into the submeridian permeable zone that extends from the Arshan resort to the south through the volcanoes of the central part of the Khamar-Daban zone and the Dzhida valley [72]. There is a decision of the tectonic reconstructions that the Khamar-Daban crust represents the thrust from Mongolia to the northern area [73, 74]. The mantle diapir should stop reaching the bottom of the thrust.

The variations in the mineral composition of the deep-seated inclusions of volcanics in TKVZ confirm the conclusions about the structure of the mantle and Moho. In the center of the rift valley, the Pl-pyroxenites are widespread, occurring in streams and dikes in the Khobok River and groups to the south of Arshan. The spinel-type peridotites and mantle begin to prevail further south; first in the Margasan flows and then in the Central Khamar-Daban volcanoes, symplectites and garnet remnants are found, which disappear into flows of the southern Khamar-Daban. In the Bartoy volcanoes are dominated xenoliths of spinel lherzolites. There and in the Karierny volcano, xenoliths characterize the entire section from the granulate to the boundary of the garnet facies of the mantle.

In time, lithospheric mantle peridotites first appeared in the basal flows under the Tumusun volcano (23 Ma). Later, the extremely heated xenolith volcano Sukhoi near Lake Baikal was introduced (16–13 Ma) [13], as well as moderately depleted peridotites from the quarry volcanoes. Later, in the central part, all the deposits were removed from the bottom of the mantle. Further, plastic-deformed peridotites appeared under the influence of mantle uplift. Further, after uplift and erosion (10–12 Ma), the volcano flows capture xenoliths from the garnet facies of the mantle. And in the Margasan flow, similar xenoliths were introduced in the most recent volcanics (2 Ma). The Quaternary volcanoes of the Tunka Valley carried out the crust material mainly. At the same time, in the Dzhida zone, which is a rift-like structure superimposed on the ancient subduction zone, the H_2O-enriched lavas and xenolith in Bartoy lavas as well are derivatives of hydrous mantle. According to some authors, the H_2O and hydrous phases in the mantle may have appeared at the stage of subduction in the Early Paleozoic-Proterozoic time [15, 36, 74].

11.2. Thermobarometry and Variations of Mantle Thermal Flow and Geotherm in TKVZ

Variations in the thermal regime that have been reconstructed using mineral thermometry for xenolith show that in most locations in the TKVZ PT estimates mainly trace the rift SEA geotherm [53]. For the Tunka Valley in Khobok (Figure 7A), the pyroxenites of the lower part of the section from 1.7 GPa just refer to the SEA geotherm of the upper part. Near the Moho the temperature variations are much wider because when the magmas reach the Moho, sometimes by near-adiabatic trajectory, they are cooling down here in contact with the cold crust. Thus, the lower Moho part consists mainly of mantle magma cumulates. At the mantle-Moho boundary, the temperature range is from 1200 to 550 °C. At the crust, the temperature range is relatively lower. The xenoliths in depth range from the Moho to the base and mainly reflect the processes of differentiation of basalt melts in polybaric magmatic systems that formed a rather thick volcanic plateau in the Elovsky spur, partly covered by sediments in the rift. In mantle beneath the Karierny in Tunka valley (Figure 7C) the capturing interval is bit higher and variations of the geothermal regime is high.

It the border of the rift in Sukhoy volcano (Figure 7E) [15] in permeable zone near the Baikal the mantle geotherm is located 150 °C above the rift SEA geotherm and reached temperatures of 1350 °C, but this is not a vertically extended area.

In the central part of the TKHVZ zone, all mantle geotherms are localized near the SEAG, reflecting the trend of mantle diapir uplift and its interaction with the deep basalt. This heating at the base is visible for the central part of the ridge volcano (Figure 7B). The mantle column beneath the Margasan River dyke is more heated because it is a more recent event (2 Ma); the heating at the Gar-Sp transition is also visible (Figure 7D).

The thermal conditions in mantle column beneath the Bartoy volcanoes vary greatly (Figure 7G). There are both colder (∼150°) areas relative to SEAG and heating ∼300° above it, reflecting the process of intrusion and interactions of basalt magmas. The fractionation trend of proto-basalt melts is located at 250–200° above SEA, and this reflects the gradient of the feeder channel. In the crust the granulites are basically pretty less, ∼150° below the rift geotherm.

11.3. Variations of the Geochemistry of the Minerals and Reason Regulating Them

The geochemistry of the constituting mantle minerals is mainly determined by the partition coefficients with the partial melts for lherzolites and basalts for their derivates. The geochemistry of the constituting mantle minerals is mainly determined by the partition coefficients with the partial melts for lherzolites and basalts for their derivates. For the lherzolitic clinopyroxenes, primitive or slightly depleted REE spectra are found, practically, in all locations. But the calculated melts with the partition coefficients [75]

show differences. In the Tunka valley in the Karierny volcano, the LREE, Th, and U are enriched, but with lowered Nd and Ta (Figure 10A), suggesting that at the rift permeable zone, the lithosphere reacted with the carbonatitic melts [54, 76]. This is less visible in the flank zone in the Margasan dyke (Figure 10B) and much less in the central part of the TKVZ (Figure 10C). The lherzolitic clinopyroxenes in the Dzhida Bartoy volcanoes have a peak in U and sometimes minima in HFSE, which may be explained by the ancient subduction influence.

The spectra of the melts of rare elements of megacrysts are determined mainly by TRE distribution coefficients. But if we look at the melt's parental relationship with the KD, the pyroxenes from pyroxenites definitely reflect the processes of differentiation of basalt melts during the formation of mantle channels associated with the separation of olivines and pyroxenes at the initial stages (Figure 10C). They show varying HFSE and LILE, which became higher together with rising REE. The melts in equilibrium with the amphiboles are much more enriched in REE and LREE, especially Sr, and HFSE are fluctuating (Figure 10D).

The parental melts for garnet are more inclined in MSD, which is due to garnet; some depletion of Zr–Hf (Figure 10F). possibly is due to joint fractionation of minor amounts of zircons. Differences for melts equilibrated with megacrysts (Figure 10E) suggest that it evolved rapidly and separated from the different melt portions. The carbonate component could be involved [55, 77] at the latest stages regulating Sr and Pb peaks as well as sulfides. The spectra of melts, Ti-biotites, and feldspar are quite diverse.

11.4. The Mantle Xenoliths as the Reflectors of the Crust-mantle Structure and Geodynamic Processes in the TKVZ

Thus, the diversity of the deep xenolith top is determined mainly by the tectonic position within the TKHVZ zone. According to some authors, the similar processes are taking place within all of Transbaikal and in Mongolia [11, 15, 76, 78]. Its frontal part, the mantle xenoliths, is somewhat depleted in Al and Ti, which reflects the xenolith from the Karierny volcano possibly reflecting the features of the continental mantle. The lherzolites from the Dzhida zone. Bartoy volcanoes containing abundant H_2O-bearing minerals possibly reflect ancient subduction-related features [36]. The minerals in the center of the Khamar-Daban set of xenolith volcanoes at the beginning were more depleted and later were mainly transported from the deeper garnet facies. Similar were determined for Shavaryn-Tsaram in Mongolia [76, 78]. The mantle in the rift valleys contains a lot of cumulative xenoliths due to the possibility of the creation of the many intermediated magmatic chambers in the fractured crust. The real granulites with the abundant garnets are relatively rare and found mainly in the Karierny volcano and in the Bartoy volcanoes at the boundaries of the TKDVZ.

The ages of the zircons from tuffs 1150–1250 Ma mainly correspond to the meta-terrigenous rocks of the Shubutuiskaya Formation in the Khamar Daban zone [65]. the Th/U ratio The Th/U ratio of 0.8–0.6 of these zircons corresponds to the common magmatic rocks, mainly of the basic type. Dated granites in the Slyudyanka complex have ages of 470–515 Ma [79].

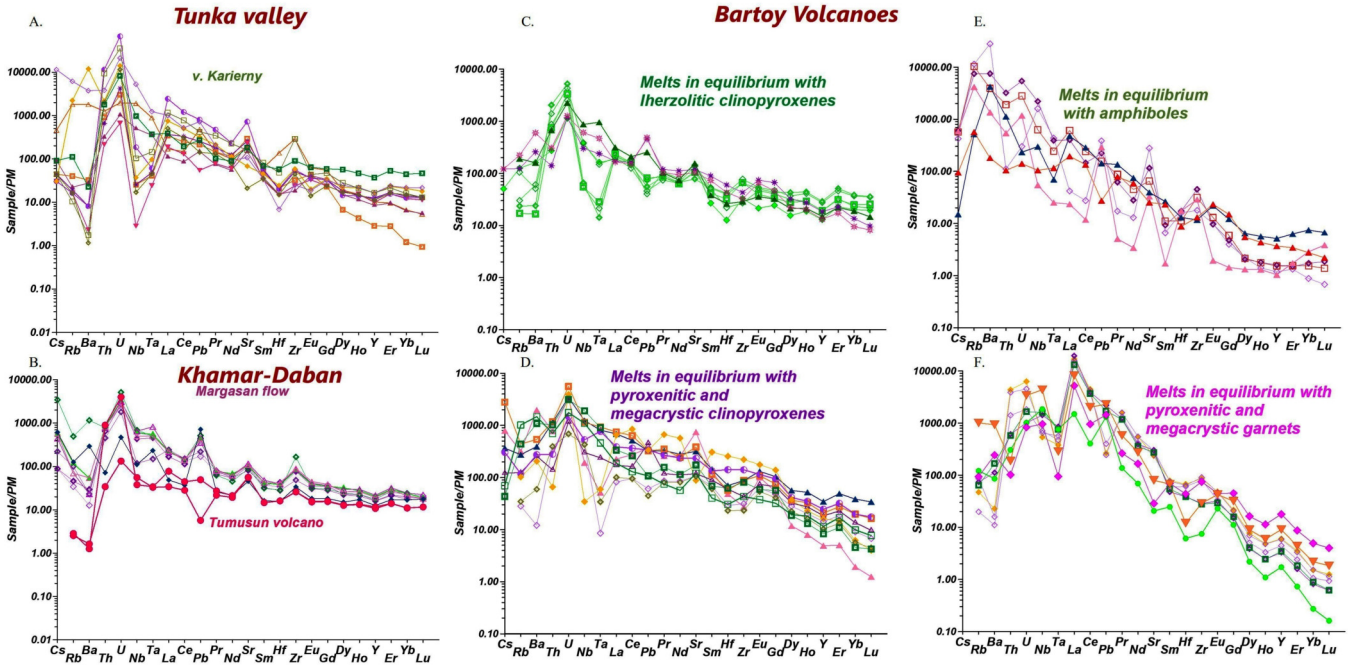

Figure 10. REE and TRE spider diagrams for the melts in equilibrium with clinopyroxenes from (**A**) Karierny volcano. (**B**) Margasan dyke and flow. (**C**) Bartoy volcanoes lherzolites. (**D**) Bartoy volcanoes pyroxenites and megacrysts. (**E**) Bartoy volcanoes amphiboles. (**F**) Bartoy volcanoes garnets.

Commonly the Khamar-Daban and Dzhida terrains are referring to the microplates. And the later terrain is thrusted over the Khamar-Daban [65]. The collision events at the boundaries of the Paleoasian ocean occurred in the Vend-Cambrian [69, 80–82] and appeared mainly in Dzhida zone. The Neoproterozoic ages which we detected here 810–870 Ma were detected everywhere within the TKHVZ and these events corresponds to the volcanic and collision processes accompanied by the metamorphism. Though some plutons with the model ages 1100–800 Ma were suggested by some authors to be referred to the collision events [65]. And elevated Th/U ratios of two zircons, 1.6–1.1, commonly correspond to the granites with the admixture of material of island arc environment with 3–5 Th/U ratios [83]. More ancient 1170–1265 Ma are more typical for the Khamar-Daban for Gar-Biotite shists and gneisses of Kornilovskaya formation [65] then for southern border where we found them. And this probably suggest the deeper zones of the crust is Dzhida may be also similar to the Centrakl Khamar Daban and collision complexes are over-thrusted.

The age of granitic zircon, 300 Ma, just corresponds to the beginning of the Angaro-Vitim Batholith formation [58, 60, 84]. It may be connected to the movement of the superplume-formed kimberlites in Yakutia [85] at the interval 420–340 Ma and later created the Biryusa and Tumanshet lamproites [86–88] and later the Ingashi lamproites in Eastern Sayan ∼306–309 Ma [88]. Further movement through Khamar-Daban and interaction with the lower crust and granulites brings to the creation of alkaline granitoids of AVP [60, 62]. But the Th/U ratio is rather low, 0.07, which commonly corresponds to the metamorphic type [89]; thus, they should be from granulites possibly remelted by a plume. Over time, volcanism manifested first in the center of the TKHVZ zone and then gradually spread to the south and north, forming volcanoes of the central type in the rift basins.

The appearance of Cenozoic volcanism in a wide area from the Pacific Ocean to Transbaikalia and Mongolia was caused by the global processes [90, 91]. There is an opinion that tectonic events and volcanism are joined and that they reflect a deep subduction spreading from the Pacific sector [92], This ore widely may reflect the processes in Circum-Pacific [92]. However, the correlation of the event and the beginning of Mesozoic volcanism is associated with the collision of Hindustan and Eurasia [93]. How can you see quite a lot of ring structures on the map (Figure 1) that reflect the rise of heated mantle matter in permeable zones from beneath that suggest the spreading of a large plume? They were formed at previous tectonic stages. Cenozoic basaltic plume magmatism was manifested over vast areas not only in Central and East Asia [94, 95] but also in the Circum-Mediterranean [1, 96] and on other continents, including Africa [97], North America [98], South America [99, 100], Australia [53], and Antarctica [101, 102]. It is likely that the deep tectonic activity as well as plume processes reflect a planetary-scale phenomenon probably controlled by cosmic forces [103].

12. Conclusions

1. The mantle and crust structures in different regions TKHVZ are rather different. The Central part contain mainly more ancient volcanites (>10–23 Ma) with the xenoliths from lherzolitic mantle lithosphere reflecting diapiric upwelling. The material is close geochemically to the primitive mantle.
2. The rifted areas at Tunka valley in more yang volcanics (to 0.5 Ma) contains mainly pyroxenitic materials from the stratified magmatic chambers and more rare granulitic material.
3. The xenolithic material from Dzhida is varying from depleted to enriched lherzolites and hydrated (probably in collision stage) with the high amount of Phl in Amph in mantle and xenocrystic—cumulative material which is accompanied by the appearance of pyrope almandine cumulative garnetsHigh var and megacrysts.
4. The high heating and vast PT ranges are typical for the bordering zone of the Baikal rift in Sykhoy and Karierny volcanoes.
5. The appearance of the water in mantle is accompanied by the deep differentiation of the basaltic mely]ts with the LILE enrichments and high variations of La/Yb and HFSE.
6. The zircon ages corresponds to the 3 intervals: 1—plume related AngaroVitim Batholiths (300 Ma); 2—collision related Vend Neoproterozoic event (810–870 Ma); 3—thrusting and metamorphic collision of microplates (1170–1265 Ma).

Supplementary Materials

The supporting information can be downloaded at: https://media.sciltp.com/articles/others/26031010232722 46/ESRS-25110106-Supplementary-Materials.zip

Author Contributions

I.A.: Writing—review & editing, Writing—original draft, Data curation, Visualization, Supervision, Resources, Validation, Software, Project administration, Methodology, Investigation, Formal analysis, Conceptualization. A.T.: Investigation, Data curation; Funding acquisition. G.B.: Investigation, Data curation. A.T.: Resources, Validation, Investigation, Conceptualization. Investigation, Data curation; Funding acquisition. T.N.: Validation, Investigation, Resources. S.R.: Conceptualization. Investigation, Data curation. I.C.: Conceptualization. Investigation, Data curation. Y.A.: Conceptualization. Investigation, Data curation. All authors have read and agreed to the published version of the manuscript.

Funding

Work is the supported by Russian Science Foundation grant 24-27-00411.

Institutional Review Board Statement

Not applicable.

Informed Consent Statement

Not applicable.

Data Availability Statement

All datasets shown in this work is a mainly analyzed just before the writing of article but it presented also in the cited articles containing the public archive information.

Acknowledgments

Work is the supported by the Ministry of Science and Higher Education of the Russian Federation and. Work was done on state assignments of IGM SB RAS FWZN-2026-0007 and Geological institute SB RAS Ulan-Ude.

Conflicts of Interest

The authors declare that they have no known competing financial interests or personal relationships that could have appeared to influence the work reported in this paper.

Use of AI and AI-assisted Technologies

During the preparation of this work, the authors used Grammar Checker and QuillBot and Grammarly English correction Tool. After that, the authors reviewed and edited the content as needed and take full responsibility for the content of the publication.

Abbreviations

SB RAS	Siberian branch of Russian Academy of Sciences
TKDVZ	Trans-Khamar Daban volcanic zone
XRF	Infra Red Spectroscopy
EPMA	Electron Probe Microanalysis
LA ICP-MS	Inductively coupled mass spectrometry with laser ablation
SEM	Secondary Electron Microscope Analyses
REE	Rare Earth Elements
LREE	Light Rare Earth Elements
REE	Heavy Rare Earth Elements
TRE	Trace Elements
Opx	Orthopyroxene
CPx	Clinopyroxene
Ol	Olivine
Cr–Sp	Chromium Spinel
Gar	Garnet
Amph	Amphibole
HFSE	High Field Strength Elements
KD	Partition Coefficient
MSD	Multicomponent Trace Element Spider Diagram

References

1. Lustrino, M.; Wilson, M. The circum-mediterranean anorogenic cenozoic igneous province. *Earth Sci. Rev.* **2007**, *81*, 1–65. https://doi.org/10.1016/j.earscirev.2006.09.002
2. Okamura, S.; Martynov, Y.A.; Furuyama, K.; et al. K–Ar ages of the basaltic rocks from Far East Russia: Constraints on the tectono-magmatism associated with the Japan Sea opening. *Isl. Arc* **1998**, *7*, 271–282. https://doi.org/10.1046/j.1440-1738.1998.00174.x
3. Martynov, Y.A.; Golozubov, V.V.; Khanchuk, A.I. Mantle diapirism at convergent boundaries (Sea of Japan). *Russ. Geol. Geophys.* **2016**, *57*, 745–755. https://doi.org/10.1016/j.rgg.2015.09.016
4. Akinin, V.V.; Roden, M.F.; Francis, D.; et al. Compositional and thermal state of the upper mantle beneath the Bering Sea basalt province: Evidence from the Chukchi Peninsula of Russia. *Can. J. Earth Sci.* **1997**, *34*, 789–800 https://doi.org/10.1139/e17-065
5. Silantyev, S.A.; Badyukov, D.D.; Akhmetshin, A.G.; et al. Evidence for partial melting in mantle xenoliths of spinel lherzolites of Zhokhov Island, De Long Archipelago, Eastern Arctic. *Petrology* **2025**, *33*, 81–93. https://doi.org/10.1134/S086959112470036X
6. Pan, M.; Yang, T.; Le, B.M.; et al. The magmatic patterns formed by the interaction of the Hainan mantle plume and Lei–Qiong crust revealed through seismic Ambient noise imaging. *Geosciences* **2024**, *14*, 63. https://doi.org/0.3390/geosciences14030063
7. Yarmolyuk, V.V.; Kuzmin, M.I.; Ernst, R.E. Intraplate geodynamics and magmatism in the evolution of the Central Asian Orogenic Belt. *J. Asian Earth Sci.* **2014**, *93*, 158–179. https://doi.org/10.1016/j.jseaes.2014.07.004
8. Martynov, Y.A.; Khanchuk, A.I.; Grebennikov, A.V.; et al. Late mesozoic and cenozoic volcanism of the East Sikhote-Alin area (Russian Far East): A new synthesis of geological and petrological data. *Gondwana Res.* **2017**, *47*, 358–371. https://doi:10.1016/j.gr.2017.01.005
9. Emelyanova, T.A.; Petrishchevsky, A.M.; Izosov, L.A.; et al. Late mesozoic–cenozoic stages of volcanism and geodynamics of the sea of Japan and sea of Okhotsk. *Petrology* **2020**, *28*, 418–430.
10. Ionov, D.A.; Prikhodko, V.S.; Bodinier, J.L.; et al. Lithospheric mantle beneath the south-eastern Siberian craton: Petrology of peridotite xenoliths in basalts from the Tokinsky Stanovik. *Contrib. Mineral. Petrol.* **2005**, *149*, 647–665. https://doi.org/10.1007/s00410-005-0672-9
11. Rasskazov, S.V.; Boven, A.; Andre, L.; et al. The evolution of magmatism in the northeastern Baikal Rift System. *Petrologiya* **1997**, *5/2*, 115–136.
12. Ashchepkov, I.V.; Tsygankov, A.A.; Burmakina, G.N.; et al. Thermal state and nature of the lower crust in the Baikal Rift Zone: Insight from xenoliths of Cenozoic and Paleozoic magmatic rocks. *Geosyst. Geoenviron.* **2024**, *3*, 100305. https://doi.org/10.1016/j.geogeo.2024.100305
13. Ashchepkov, I.V.; Travin, S.V.; Saprykin, A.I.; et al. Age of xenolith-bearing basalts and mantle evolution in the Baikal rift zone. *Russ. Geol. Geophys.* **2003**, *44*, 1160–1188.
14. Ashchepkov, I.V.; Andre, L.; Downes, H.; et al. Pyroxenites and megacrysts from Vitim picrite-basalts (Russia): Polybaric fractionation of rising melts in the mantle? *J. Asian Earth Sci.* **2011**, *42*, 14–37. https://doi.org/10.1016/j.jseaes.2011.03.004
15. Ashchepkov, I.V. *Deep Xenoliths of the Baikal Rift*; Nauka, Siberian Branch: Novosibirsk, Russia, 1991; p. 160.
16. Chien, Y.H.; Wang, K.L.; Kovach, V.; et al. Geochemical characteristics of peridotite xenoliths from the Vitim volcanic field: Insight to late Cenozoic mantle upwelling in SE Siberia. *Lithos* **2024**, *482*, 107727.
17. Glaser, S.M.; Foley, S.F.; Günther, D. Trace element compositions of minerals in garnet and spinel periodotite xenoliths from the Vitim volcanic field, Transbaikalia, eastern Siberia. *Dev. Geotectonics* **1999**, *24*, 263–285. https://doi.org/10.1016/S0419-0254(99)80015-9
18. Kiselev, A.I.; Medvedev, M.E.; Golovko, G.A. *Volcanism of the Baikal Rift Zone and Problems of Deep Magma Formation*; Nauka, Siberian Branch: Novosibirsk, Russia, 1979; p. 205
19. Grachev, A.F. Khamar-Daban a hotspot of the Baikal Rift according to chemical geodynamics. *Phys. Earth* **1998**, *34*, 28–48.
20. Rasskazov, S.V.; Bogdanov, G.V.; Medvedeva, T.I.; et al. Deep-

seated xenoliths from the Bartoy volcanics (West Transbaikalia). *Volkanol. Seismol.* **1989**, *3*, 38–48. (In Russian)

21. Rasskazov, S.V. *Magmatism of the Baikal Rift System*; Nauka: Novosibirsk, Russia, 1993; p. 286.
22. Yarmolyuk, V.V.; Kozlovsky, A.M.; Savatenkov, V.M.; et al. Early mesozoic bimodal volcanic sequences of central Mongolia: Implications for the evolution of the khentey segment of the Mongol–Okhotsk Belt. *Petrology* **2024**, *32*, 804–827. https://doi.org/10.1134/S0869591124700206
23. Krylov, S.V.; Mishenkin, B.P.; Bryskin, A.V. Deep structure of the Baikal rift from multiwave seismic explorations. *J. Geodyn.* **1991**, *13*, 87–96. https://doi.org/10.1016/0264-3707(91)90032-A
24. Belichenko, V.G.; Gelety, N.K.; Barash, I.G. The Barguzin microcontinent (Baikal mountain region): The recognizing problem. *Russ. Geol. Geophys.* **2006**, *47*, 1049–1059.
25. Kulakov, I.Yu. Three-dimensional seismic heterogeneities beneath the Baikal region according to data of local teleseismic tomography. *Russ. Geol. Geophys.* **1999**, *40*, 317–331.
26. Zorin, Yu.A.; Turutanov, E.Kh. Regional isostatic gravity anomalies and mantle plumes in southern East Siberia (Russia) and Central Mongolia, *Russ. Geol. Geophys.* **2004**, *45*, 1248–1258.
27. Kiselev, A.I.; Popov, A.M. Asthenospheric diapir beneath the Baikal rift: Petrological constraints. *Tectonophysics* **1992**, *208*, 287–295. https://doi.org/10.1016/0040-1951(92)90350-F
28. Savatenkov, V.M.; Yarmolyuk, V.V.; Kudryashova, E.A.; et al. Sources and geodynamics of the Late Cenozoic volcanism of Central Mongolia: Evidence from isotope-geochemical studies. *Petrology* **2010**, *18*, 278–307. https://doi.org/10.1134/S0869591110030057
29. Ivanov, A.V.; Arzhannikov, S.G.; Demonterova, E.I.; et al. Jom-Bolok Holocene volcanic field in the East Sayan Mts.; Siberia, Russia: Structure, style of eruptions, magma compositions, and radiocarbon dating. *Bull. Volcanol.* **2011**, *73*, 1279–1294. https://doi.org/10.1007/s00445-011-0485-9
30. Yarmolyuk, V.V.; Kozlovsky, A.M.; Kuzmin, M.I. Zoned magmatic areas and anorogenic batholith formation in the Central Asian Orogenic Belt (by the example of the Late Paleozoic Khangai magmatic area). *Russ. Geol. Geophys.* **2016**, *57/3*, 357–370. https://doi:10.1016/j.rgg.2016.03.001
31. Ailow. Y. 2022. Deep-seated inclusions from Cenozoic volcanic rocks in the Tunka Valley of the Baikal Rift System in the structure of the Early Paleozoic Slyudyanka metamorphic complex. In *Dissertation for the Scientific Degree of Candidate of Geological and Mineralogical Sciences*; Institute of the Earth Crust, Siberian Branch of Russian Academy of Sciences: Irkutsk, Russia, 2022; p. 254
32. Ailow, Y.; Rasskazov S.V.; Chuvashova, I.S.; et al. Relationship between rocks of primitive mantle, restites, and metasomatites in inclusions from basanites of the Karierny Volcano (Western Pribaikal). Izvestiya Irkutsk State University. *Izv. Irkutsk. State Univ., Ser. Earth Sci.* **2019**, 29, 3–23. https://doi.org/10.26516/2073-3402.2019.29.3
33. Ionov, D.A.; O'Reilly, S.Y.; Ashchepkov, I.V. Feldspar-bearing lherzolite xenoliths in alkali basalts from Hamar-Daban, southern Baikal region, Russia. *Contrib. Mineral. Petrol.* **1995**, *122*, 174–190. https://doi.org/10.1007/s004100050120
34. Gornova, M.A.; Belyaev, V.A.; Karimov, A.A.; et al. Chemical Modification of lherzolite xenoliths due to interaction with host basanite melt: Evidence from Tumusun Volcano, Baikal Rift Zone. *Minerals* **2023**, *13*, 403. https://doi.org/10.3390/min13030403
35. Melyakhovetsky, A.A.; Ashchepkov, I.V.; Dobretsov, N.L. Amphibole-and phlogopite-bearing mantle xenoliths and co-magmatic inclusions from paleovolcanoes of the Bartoy volcano group, Baikal rift zone. *Doklady Earth Sci.* **1989**, *286*, 163–167.
36. Ionov, D.A.; Kramm, U.; Stosh, H.-G. Evolution of the upper mantle beneath the southern Baikal rift zone: An Sm–Nd isotope study of xenoliths from the Bartoy volcanoes. *Contrib. Miner. Petrol.* **1992**, *111*, 235–247. https://doi.org/10.1007/BF0034895430
37. Ivanov, A.V.; Demonterova, E.I. Extension in the Baikal rift and the depth of basalt magma generation. *Dokl. Earth Sci.* **2010**, *435*, 1564. https://doi.org/10.1134/S1028334X10120032
38. Lavrent'ev, Y.G.; Korolyuk, V.; Usova, L.; et al. Electron probe microanalysis of rock-forming minerals with a JXA-8100 electron probe microanalyzer. *Russ. Geol. Geophys.* **2015**, *56*, 1428–1436. https://doi.org/10.1016/j.rgg.2015.09.005
39. Wilshire, H.C.; Shervais, J.W. Al-augite and Cr-diopside ultramafic xenoliths in basaltic rocks from Western United States. *Phys. Chem. Earth* **1975**, *9*, 257–272. https://doi.org/10.1016/B978-0-08-018017-5.50024-9
40. Sláma, J.; Košler, J.; Condon, D.J.; et al. Plešovice zircon—A new natural reference material for U–Pb and Hf isotopic microanalysis. *Chem. Geol.* **2008**, *249*, 1–35. https://doi.org/10.1016/j.chemgeo.2007.11.005
41. Huang, C.; Wang, H.; Yang, J.H.; et al. SA01–A proposed zircon reference material for microbeam U-Pb age and Hf-O isotopic determination. *Geostand. Geoanal. Res.* **2020**, *44*, 103–123. https://doi.org/doi.org/10.1111/ggr.12307
42. Gain, S.E.; Gréau, Y.; Henry, H.; et al. Mud tank zircon: Long-term evaluation of a reference material for U-pb dating, hf-isotope analysis and trace element analysis. *Geostand. Geoanal. Res.* **2019**, *43*, 339–354. https://doi.org/10.1111/ggr.12265
43. Ludwig, K.R. User's manual for Isoplot 3.75: A geochronological toolkit for Microsoft Excel. *Berkeley Geochronol. Cent. Spec. Publ.* **2012**, *5*, 75.
44. Leake, B.E.; Woolley, A.R.; Arps, C.E.S.; et al. Nomenclature of amphiboles: Report of the subcommittee on amphiboles of the international association, commission on new minerals and mineral names. *Am. Mineral.* **1997**, *82*, 1019–1037.
45. Brey, G.P.; Köler, T. Geothermobarometry in four-phase lherzolites II. New thermobarometers and practical assessment of existing thermobarometers. *J. Petrol.* **1990**, *31*, 1353–1378. https://doi.org/10.1093/petrology/31.6.1353
46. Newton, R.C.; Perkins, D. Thermodynamic calibration of geobarometers based on the assemblages garnet-plagioclase-orthopyroxene (clinopyroxene)-quartz. *Am. Mineral.* **1982**, *67*, 203–222.
47. Nimis, P.; Taylor, W. Single clinopyroxene thermobarometry for garnet peridotites. Part I. Calibration and testing of a Cr-in-Cpx barometer and an enstatite-in-Cpx thermometer. *Contrib. Mineral. Petrol.* **2000**, *139*, 541–554. https://doi.org/10.1007/s004100000156
48. Ashchepkov, I.V.; Ntaflos, T.; Logvinova, A.M.; et al. Monomineral universal clinopyroxene and garnet barometers for peridotitic, eclogitic and basaltic systems. *Geosci. Front.* **2017**, 8, 775–795. https://doi.org/10.1016/j.gsf.2016.06.012
49. Krogh, E.J. The garnet-clinopyroxene Fe-Mg geothermometer — A reinterpretation of existing experimental data. *Contrib. Mineral. Petrol.* **1988**, *99*, 44-48, https://doi.org/10.1007/BF00399364
50. Ravna E.K. Distribution of Fe2+ and Mg between coexisting garnet and hornblende in synthetic and natural systems: An empirical calibration of the garnet-hornblende Fe-Mg geothermometer. *Lithos* **2000**, *53*, 265–277. https://doi.org/10.1016/S0024-4937(00)00029-3
51. Ashchepkov, I.V.; Babushkina, S.A.; Kostrovitsky, S.I.; et al. Mantle amphiboles from the lithospheric keel of the Siberian Craton: Reconstructions using new thermobarometry and geochemistry. *Geosyst. Geoenviron.* **2025**, *4*, 100427. https://doi.org/10.1016/j.geogeo.2025.100427
52. Pollack, H.N.; Chapman, D.S. On the regional variation of heat fow, geotherms and lithospheric thickness. *Tectonophysics* **1977**, *38*, 279–296. https://doi.org/10.1016/0040-1951(77)90215-3
53. O'Reilly, S.Y.; Griffin W.L. A xenolith-derived geotherm from southeastern Australia and its geophysical implications. *Tectonophysics* **1985**, *111*, 41–63. https://doi.org/10.1016/0040-1951(85)90065-4

54. McDonough, W.F.; Sun, S.S. The Composition of the Earth. *Chem. Geol.* **1995**, *120*, 223–253. https://doi.org/10.1016/0009-2541(94)00140-4
55. Rudnick, R.L.; McDonough, W.F.; Chappell, B.W. Carbonatite metasomatism in the northern Tanzanian mantle: Petrographic and geochemical characteristics. *Earth Planet. Sci. Lett.* **1993**, *114*, 463–475. https://doi.org/10.1016/0012-821X(93)90076-L
56. Tsygankov, A.A.; Litvinovsky, B.A.; Jahn, B.M.; et al. Complex sequence of magmatic events in the late palaeozoic of Transbaikalia, Russia (U–Pb isotope data). *Russ. Geol. Geophys.* **2010**, *51*, 901–922. https://doi/10.1016/j.rgg.2010.08.007
57. Yarmolyuk, V.V.; Kuzmin, M.I. Late Paleozoic and Early Mesozoic rare-metal magmatism of Central Asia: Stages, provinces, and formation settings. *Geol. Ore Depos.* **2012**, *54*, 313–333. https://doi/10.1134/s1075701512050054
58. Tsygankov, A.A.; Burmakina, G.N.; Khubanov, V.B.; et al. Geodynamics of late Paleozoic Batholith-Forming processes in Western Transbaikalia. *Petrology* **2017**, *25*, 396–418. https://doi.org/10.1134/s0869591117030043
59. Yarmolyuk, V.V.; Kuzmin, M.I.; Kozlovsky, A.M. Late paleozoic-early Mesozoic within-plate magmatism in North Asia: Traps, rifts, giant batholiths, and the geodynamics of their origin. *Petrology* **2013**, *21*, 101–126. https://doi.org/10.1134/S0869591113010062
60. Tsygankov, A.A.; Khubanov, V.B.; Burmakina, G.N.; et al. Frequency of endogenous events in western transbaikalia and northern Mongolia (eastern segment of the Central Asian Orogenic Belt) according to U–Pb dating of detrital zircon grains from modern fluvial deposits. *Strat. Geol. Correl.* **2023**, *31*, 355–375. https://doi.org/10.31857/S0869592X23050083
61. Tsygankov, A.A.; Burmakina, G.N.; Khubanov, V.B.; et al. Nd isotope systematics of Late Paleozoic granitoids from the Western Transbaikalia (Russia): Petrological consequences and plume model testing. *Geosyst. Geoenviron.* **2024**, *3*, 100266. https://doi.org/10.1016/j.geogeo.2024.100266
62. Jahn, B.M.; Litvinovsky, B.A.; Zanvilevich, A.N.; et al. Peralkaline granitoid magmatism in the Mongolian–Transbaikalian Belt: Evolution, petrogenesis and tectonic significance. *Lithos* **2009**, *113*, 521–539. https://doi.org/10.1016/j.lithos.2009.06.015
63. Lykhin, D.A.; Yarmolyuk, V.V. Magmatism and formation conditions of the Urma helvite-bertrandite deposit, West Transbaikal berillium province. *Geol. Ore Depos.* **2014**, *56*, 281–301. https://doi.org/10.1134/s1075701514040059
64. Shkol'nik, S.I.; Stanevich, A.M.; Reznitskii, L.Z.; et al. New data about structure and time of formation of the Khamar-Daban terrane: U-Pb LA-ICP-MS zircon ages. *Stratigr. Geol. Correl.* **2016**, *24*, 19–38. https://doi.org/10.1134/S086959381506009X
65. Gordienko, I.V.; Kovach, V.P.; Elbaev, A.L.; et al. Collisional granitoids of the Dzhida zone of the central Asian fold belt, Southwestern Transbaikalia: Age and conditions of the formation. *Petrology* **2012**, *20*, 40–58. https://doi.org/doi:10.1134/s086959111201002x
66. Delvaux, D.; Moeys, R.; Stapel, G.; et al. Paleostress reconstruction and geodynamics of the Baikal region, Central Asia. Part I: Paleozoic and Mesozoic prerift evolution. *Tectonophysics* **1995**, *252*, 61–101. https://doi.org/10.1016/0040-1951(95)00090-9
67. Suvorov, V.D.; Mishenkina, Z.M.; Petrick, G.V,; et al. Structure of the crust in the Baikal rift zone and adjacent areas from Deep Seismic Sounding data. *Tectonophysics* **2002**, *351*, 61–74. https://doi.org/10.1016/S0040-1951(02)00125-7
68. Gordienko, I.V.; Geodynamic evolution of late Baikalides and Paleozoids in the folded periphery of the Siberian craton. *Russ. Geol. Geophys.* **2006**, *47*, 53–70.
69. Byzov, L.; Sankov, V. The evolution of continental rifts revealed from the numerical modeling: A case study of the Baikal rift system, Siberia. *J. Asian Earth Sci.* **2024**, *259*, 105871. https://doi.org/10.1016/j.jseaes.2023.105871
70. Zorin, Y.A.; Novoselova, M.R.; Turutanov, E.K.; et al. Structure of the lithosphere of the Mongolian-Siberian mountainous province. *J. Geodynam.* **1990**, *11*, 327–342. https://doi.org/10.1016/0264-3707(90)90015-M
71. Pospeeva, E.; Duchkov, A.; Potapov, V.; et al. Lithosphere of the West Transbaikalian sector of the Central Asian fold belt according to electromagnetic studies. In *Heat-Mass Transfer and Geodynamics of the Lithosphere*; Springer International Publishing: Cham, Switzerland, 2021; pp. 351–380. https://doi.org/10.1007/978-3-030-63571-8_20*
72. Reznitsky, L.Z.; Barash, I.G.; Kovach, V.P.; et al. Paleozoic intrusive magmatism of the Dzhida terrane – New geochronological and Nd isotope data. In *Geodynamic Evolution of the Lithosphere of the Central Asian Mobile Belt (from Ocean to Continent)*; IEC SB RAS; Irkutsk, Russia, 2005; Volume 3, pp. 77–80. (In Russian)
73. Yarmolyuk, V.V.; Kuzmin, M.I.; Kozlovsky A.M. Late paleozoic-early mezozoic within-plate magmatism in north asia: Traps, rifts, giant batholiths, and the geodynamics of their origin. *Petrology* **2013**, *21*, 101–125. https://doi.org/doi:10.1134/s0869591113010062
74. Al'muhamedov, A.I.; Gordienko, I.V.; Kuzmin, M.I.; et al. The Dzhida zone: A fragment of the Paleoasian ocean. *Geotectonics* **1996**, *4*, 25–42.
75. Hart, S.R.; Dunn, T. Experimental clinopyroxene/melt partitioning of 24 trace elements. *Contrib. Mineral. Petrol.* **1993**, *113*, 1–8. https://doi.org/10.1007/BF00320827
76. Kourim, F.; Wang, K.-L.; Beinlich, A.; et al. Metasomatism of the off-cratonic lithospheric mantle beneath Hangay Dome, Mongolia: Constraints from trace-element modelling of lherzolite xenoliths. *Lithos* **2021**, 400–401, 106407. https://doi.org/10.1016/j.lithos.2021.106407
77. Coltorti, M.; Bonadiman, C.; Hinton, R.W.; et al. Carbonatite metasomatism of the oceanic upper mantle: Evidence from clinopyroxenes and glasses in ultramafic xenoliths of Grande Comore, Indian Ocean. *J. Petrol.* **1999**, *40*, 133–165. https://doi.org/10.1093/petroj/40.1.133
78. Kopylova, M.G.; O'Reilly, S.Y.; Genshaft, Y.S. Thermal state of the lithosphere beneath Central Mongolia: Evidence from deep-seated xenoliths from the Shavaryn-Saram volcanic centre in the Tariat depression, Hangai, Mongolia. *Lithos* **1995**, *36*, 243–255. https://doi.org/10.1016/0024-4937(95)00020-8
79. Barash, I.G.; Sal'nikova, E.B.; Reznitskii, L.Z.; et al. Age relations between metamorphism of the Slyudyanka granulite and the Khamar-Daban zoned metamorphic complexes: Evidence from U–Pb geochronological data, *Dokl. Earth Sci.* **2006**, 905–908. https://doi.org/10.1134/s1028334x06060158
80. Gordienko, I.V. Relationship between subduction-related and plume magmatism at the active boundaries of lithospheric plates in the interaction zone of the Siberian continent and Paleoasian Ocean in the Neoproterozoic and Paleozoic. *Geodyn. Tectonophys.* **2019**, *10*, 405–457. https://doi.org/10.1016/j.rgg.2016.01.005
81. Mazukabzov, A.M.; Donskaya, T.V.; Gladkochub, D.P.; et al. The Late Paleozoic geodynamics of the West Transbaikalian segment of the Central Asian fold belt. *Russ. Geol. Geophys.* **2010**, *51*, 482–491. https://doi.org 10.1016/j.rgg.2010.04.008
82. Donskaya, T.V.; Gladkochub, D.P.; Mazukabzov, A.M.; et al. Late Paleozoic–Mesozoic subduction-related magmatism at the southern margin of the Siberian continent and the 150 million-year history of the Mongol-Okhotsk Ocean. *J. Asian Earth Sci.* **2013**, *62*, 79–95. https://doi.org/10.1016/j.jseaes.2012.07.023
83. Hawkesworth, C.; Turner, S.; Peate, D.; et al. Elemental U and Th variations in island arc rocks: Implications for U-series isotopes. *Chem. Geol.* **1997**, *139*, 207–221. https://doi.org/10.1016/S0009-2541(97)00036-3
84. Khubanov, V.B.; Tsygankov, A.A.; Burmakina, G.N. Duration and formation geodynamics of the Angara-Vitim batholith: Data of U-Pb LA-ICP-MS isotope dating of magmatic and detrital zircons. *Russ. Geol. Geophys.* **2021**, *62*, 1331–1349. https://doi.org/10.2113/RGG20204223

85. Kostrovitsky, S.I.; Yakovlev, D.A.; Fosu, B.R.; et al. A geological, geochemical and isotopic study of primary diamond deposits in the Siberian craton. *Miner. Petrol.* **2025**, *119*, 21–47. https://doi.org/10.1007/s00710-024-00880-3

86. Sun, J.; Tappe, S.; Kostrovitsky, S.I.; et al. Mantle sources of kimberlites through time: A U-Pb and Lu-Hf isotope study of zircon megacrysts from the Siberian diamond fields. *Chem. Geol.* **2018**, *479*, 228–240. https://doi.org/10.1016/j.chemgeo.2018.01.013

87. Egorov, K.N.; Kiselev, A.I.; Men'shagin, Y.V.; et al. Lamproite and kimberlite of the Sayany area: Composition, sources, and diamond potential. *Dokl. Earth Sci.* **2010**, *435*, 1670–1675. https://doi.org/10.1134/S1028334X10120251

88. Gladkochub, D.P.; Kostrovitskii, S.I.; Donskaya, T.V.; et al. Age of zircons from diamond-bearing lamproites of the East Sayan as an indicator of known and unknown endogenous events in the south Siberian Craton. *Dokl. Earth Sci.* **2013**, *450*, 567–572. https://doi.org/doi:10.1134/s1028334x1306010x

89. Barry, T.L.; Saunders, A.D.; Kempton, P.D.; et al. Petrogenesis of Cenozoic Basalts from Mongolia: Evidence for the role of asthenospheric versus metasomatized lithospheric mantle sources. *J. Petrol.* **2003**, *44*, 55–91. https://doi.org/10.1093/petrology/44.1.55

90. Trifonov, V.G.; Sokolov, S.Y.; Bachmanov, D.M. et al. Neotectonics and the Upper Mantle Structure of Central Asia. *Geotectonics* **2021**, *55*, 334–360. https://doi.org/10.1134/S0016852121030080

91. Chekhovich, V.D.; Palandzhyan, S.A. Late cretaceous Okhotsk–Penzhina–Anadyr small oceanic basin (Northeast Eurasia): Geological evidence and geodynamic evolution. *Geotectonics* **2024**, *58*, 477–499. https://doi.org/10.1134/S0016852124700353

92. Kennett, J.P.; McBirney, A.R.; Thunell, R.C. Episodes of Cenozoic volcanism in the circum-Pacific region. *J. Volcanol. Geotherm. Res.* **1977**, *2*, 145–163. https://doi.org/10.1016/0377-0273(77)90007-5

93. Sokolov, S.Y.; Trifonov, V.G. Arc tectonic elements and upper mantle structure of Central and Southeast Asia: Seismic tomography and seismicity data. *Geotectonics* **2024**, *58*, 23–40. https://doi.org/10.1134/S001685212470002X

94. Choi, S.H.; Mukasa, S.B.; Zhou, X.-H.; et al. Mantle dynamics beneath East Asia constrained by Sr, Nd, Pb and Hf isotopic systematics of ultramafic xenoliths and their host basalts from Hannuoba, North China. *Chem. Geol.* **2008**, *248*, 40–61. https://doi.org/10.1016/j.chemgeo.2007.10.008

95. Wickham, S.M.; Litvinovsky, B.A.; Zanvilevich, A.N.; et al. Geochemical evolution of phanerozoic magmatism in Transbaikalia, East Asia: A key constraint on the origin of K-rich silicic magmas and the process of cratonization. *J. Geophys. Res. Solid Earth* **1995**, *100*, 15641–15654. https://doi.org/10.1029/95JB00035

96. Harangi, S.; Jankovics, M.É.; Sági, T.; et al. Origin and geodynamic relationships of the late miocene to quaternary alkaline basalt volcanism in the Pannonian basin, eastern–central Europe. *Int. J. Earth Sci. (Geol. Rundsch)* **2015**, *104*, 2007–2032. https://doi.org/10.1007/s00531-014-1105-7

97. Whattam, S.A.; Azizi, H.; Iskandar, O.; et al. Asymmetrical magma chamber beneath the Red Sea system controlled Cenozoic alkaline magmatism on the western margin of the Arabian Shield. *J. Geol. Soc.* **2025**, *182*, jgs2024-280. https://doi.org/10.1144/jgs2024-280

98. Farmer, G.L. Reassessing the role of continental lithospheric mantle in Cenozoic magmatism, southwestern North America. *Isot. Constraints Earth Syst. Process.* **2022**, 57–86. https://doi.org/10.1002/9781119595007.ch4

99. de Souza, Z.S.; Vilalva, F.C.J.; Lafon, J.M.; et al. Geochemistry and Sr–Nd–Pb isotope geology of intraplate Cenozoic basaltic volcanism of NE Brazil: Remnant of an aborted mid-ocean ridge? *Contrib. Mineral. Petrol.* **2025**, *180*, 18. https://doi.org/10.1007/s00410-025-02207-7

100. Ferreira, L.C.; Stanton, N.; Gordon, A.C.; et al. The magmatic rifting of Santos Basin: Aeromagnetic mapping of dykes, terranes and marginal structures and the interplay between tectonism and volcanism. *Tectonics* **2023**, *42*, e2022TC007560. https://doi.org/10.1029/2022TC007560

101. Andronikov, A.V.; Andronikova, I.E.; Sidorinova, T. Trace-element geochemistry of sulfides in upper mantle lherzolite xenoliths from East Antarctica. *Minerals* **2021**, *11*, 773. https://doi.org/10.3390/min11070773

102. Panter, K.S.; Li, Y.; Smellie, J.L.; et al. Mantle sources and melting processes beneath East Antarctica: Geochemical and isotopic (Sr, Nd, Pb, O) characteristics of alkaline and tholeiite basalt from the Earth's southernmost (87° S) volcanoes. *Contrib. Mineral. Petrol.* **2022**, *177*, 51. https://doi.org/10.1007/s00410-022-01914-9

103. Rampino, M.R.; Caldeira, K.; Rodriguez, S. Cycles of ∼32.5 My and ∼26.2 My in correlated episodes of continental flood basalts (CFBs), hyper-thermal climate pulses, anoxic oceans, and mass extinctions over the last 260 My: Connections between geological and astronomical cycles. *Earth-Sci. Rev.* **2023**, *246*, 104548. https://doi.org/10.1016/j.earscirev.2023.104548